

ARMY RESEARCH LABORATORY



A Molecular Dynamics Study of Detonation: II. The Reaction Mechanism

Betsy M. Rice
William Mattson
John Grosh

U.S. ARMY RESEARCH LABORATORY

S. F. Trevino

U.S. ARMY ARMAMENT RESEARCH, DEVELOPMENT, & ENGINEERING CENTER
AND NATIONAL INSTITUTE OF STANDARDS AND TECHNOLOGY

ARL-TR-982

March 1996

APPROVED FOR PUBLIC RELEASE; DISTRIBUTION IS UNLIMITED.

19960314 066

Microfilm Edition

NOTICES

Destroy this report when it is no longer needed. DO NOT return it to the originator.

Additional copies of this report may be obtained from the National Technical Information Service, U.S. Department of Commerce, 5285 Port Royal Road, Springfield, VA 22161.

The findings of this report are not to be construed as an official Department of the Army position, unless so designated by other authorized documents.

The use of trade names or manufacturers' names in this report does not constitute indorsement of any commercial product.

REPORT DOCUMENTATION PAGE			Form Approved OMB No. 0704-0188	
Public reporting burden for this collection of information is estimated to average 1 hour per response, including the time for reviewing instructions, searching existing data sources, gathering and maintaining the data needed, and completing and reviewing the collection of information. Send comments regarding this burden estimate or any other aspect of this collection of information, including suggestions for reducing this burden, to Washington Headquarters Services, Directorate for Information Operations and Reports, 1215 Jefferson Davis Highway, Suite 1204, Arlington, VA 22202-4302, and to the Office of Management and Budget, Paperwork Reduction Project(0704-0188), Washington, DC 20503.				
1. AGENCY USE ONLY (Leave blank)		2. REPORT DATE March 1996		3. REPORT TYPE AND DATES COVERED Final, Jan 94 - Jul 95
4. TITLE AND SUBTITLE A Molecular Dynamics Study of Detonation: II. The Reaction Mechanism			5. FUNDING NUMBERS PR: 1L161102AH43	
6. AUTHOR(S) B. M. Rice, W. Mattson, J. Grosh, and S. F. Trevino*				
7. PERFORMING ORGANIZATION NAME(S) AND ADDRESS(ES) U.S. Army Research Laboratory ATTN: AMSRL-WT-PC Aberdeen Proving Ground, MD 21005-5066			8. PERFORMING ORGANIZATION REPORT NUMBER ARL-TR-982	
9. SPONSORING/MONITORING AGENCY NAMES(S) AND ADDRESS(ES)			10. SPONSORING/MONITORING AGENCY REPORT NUMBER	
11. SUPPLEMENTARY NOTES *U.S. Army Armament Research, Development, and Engineering Center, Picatinny Arsenal, NJ 07806, and National Institute of Standards and Technology, Gaithersburg, MD 20899.				
12a. DISTRIBUTION/AVAILABILITY STATEMENT Approved for public release; distribution is unlimited.			12b. DISTRIBUTION CODE	
13. ABSTRACT (Maximum 200 words) In this work, we investigate mechanisms of chemical reactions that sustain an unsupported detonation. The chemical model of an energetic crystal used in this study consists of heteronuclear diatomic molecules that, at ambient pressure, dissociate endothermically. Subsequent association of the products to form homonuclear diatomic molecules provides the energy release that sustains the detonation. A many-body interaction is used to simulate changes in the electronic bonding as a function of local atomic environment. The consequence of the many-body interaction in this model is that the intramolecular bond is weakened with increasing density. The mechanism of reaction for this model was extracted by investigating the details of the molecular properties in the reaction zone with two-dimensional molecular dynamics. The mechanism for initiation of reaction in this model is pressure-induced atomization. There was no evidence of excitation of vibrational modes to dissociative states. This particular result is directly attributable to the functional form and choice of parameters for this model, but might also have more general applicability.				
14. SUBJECT TERMS molecular dynamics, detonation, reaction mechanism			15. NUMBER OF PAGES 44	
			16. PRICE CODE	
17. SECURITY CLASSIFICATION OF REPORT UNCLASSIFIED	18. SECURITY CLASSIFICATION OF THIS PAGE UNCLASSIFIED	19. SECURITY CLASSIFICATION OF ABSTRACT UNCLASSIFIED	20. LIMITATION OF ABSTRACT UL	

INTENTIONALLY LEFT BLANK.

ACKNOWLEDGMENTS

The authors wish to thank Dr. John Lyons, Director of the U.S. Army Research Laboratory (ARL), for his support under the Director's Research Initiative. BMR wishes to thank Drs. Robert Frey, Douglas Kooker, and Anthony Kotlar for helpful comments. The calculations reported in this work were done on the SGI Power Challenge Array at the DOD High Performance Computing Site at ARL, Aberdeen Proving Ground, MD.

INTENTIONALLY LEFT BLANK.

TABLE OF CONTENTS

	<u>Page</u>
ACKNOWLEDGMENTS	iii
LIST OF FIGURES	vii
LIST OF TABLES	ix
1. INTRODUCTION	1
2. MODELS	3
2.1 Models 0 and I	3
2.2 Model II	13
3. DETAILS OF THE CALCULATIONS	17
4. RESULTS	20
5. CONCLUSIONS	29
6. REFERENCES	31
DISTRIBUTION LIST	33

INTENTIONALLY LEFT BLANK.

LIST OF FIGURES

Figure	Page
1. Intramolecular interaction potentials of Model 0 for different $\overline{B_{ij}}$ values (Equation 1) as functions of internuclear distance for (a) A-B interactions; (b) A-A interactions .	6
2. Snapshot of chemically sustained shock waves at 15 ps initiated by a four-layer flyer plate with an impact velocity of 6 km/s	8
3. Potential energy contours (in eV) for the following collinear three-body reactions using Model I: (a) $A + A-B \rightarrow A-A + B$; (b) $A + BA \rightarrow A-B + A$; (c) $A + A-A \rightarrow A-A + A$	9
4. Schematic of the potential energy for three-body collinear reactions (I)-(III) for Model I	12
5. Potential energy contours (in eV) for the following collinear three-body reactions using Model II: (a) $A + A-B \rightarrow A-A + B$; (b) $A + B-A \rightarrow A-B + A$; (c) $A + B-B \rightarrow A-B + B$; (d) $B + A-B \rightarrow B-A + B$; (e) $A + A-A \rightarrow A-B + A$; (f) $B + B-B \rightarrow B-B + B$	15
6. Intramolecular interaction potentials of Model II for different $\overline{B_{ij}}$ values (Equation 2) as functions of internuclear distance for (a) A-B interactions; (b) A-A interactions; and (c) B-B interactions	16
7. Normalized translational energy distributions of original A-B pairs for seven regions directly behind the shock front through the 12 km/s simulation (up to 7.8 ps)	23
8. Normalized rotational energy distributions of original A-B pairs for seven regions directly behind the shock front through the 12 km/s simulation (up to 7.8 ps)	23
9. Normalized vibrational KE distributions of original A-B pairs for seven regions directly behind the shock front through the 12 km/s simulation (up to 7.8 ps)	24
10. Normalized distribution of intramolecular terms of Equation (2) of original A-B pairs for seven regions directly behind the shock front through the 12 km/s simulation (up to 7.8 ps)	24
11. Normalized distribution of $\overline{B_{ij}}$ terms of Equation (2) of original A-B pairs for seven regions directly behind the shock front through the 12 km/s simulation (up to 7.8 ps)	25
12. Normalized distribution of internuclear distances of original A-B pairs for seven regions directly behind the shock front through the 12 km/s simulation (up to 7.8 ps)	25
13. Normalized distribution of orientation angles of original A-B pairs relative to the crystal x-axis for seven regions directly behind the shock front through the 12 km/s simulation (up to 7.8 ps)	26

INTENTIONALLY LEFT BLANK.

LIST OF TABLES

<u>Table</u>	<u>Page</u>
1. Parameters and Functional Forms Used for the Potential Energy Expressions in Equations (1) and (2)	4
2. Geometric Parameters and Harmonic Vibrational Frequencies of Critical Points on the Potential Energy Surfaces for Models 0, I, and II	11
3. Lattice Parameters, Density, and Molecular Geometries vs. Pressure for Models I and II	18
4. Averages of Properties of Unreacted A-B Molecules in Reaction Zone Throughout 12 km/s Simulation of Unsupported Detonation	22

INTENTIONALLY LEFT BLANK.

1. INTRODUCTION

Are the reactions that occur behind the shock front in a detonation due to rapid heating of molecules to dissociation after shock wave passage, or are the bonds mechanically broken after shock compression? Or do reactions result from a combination of both processes? What are the consequences for the properties of the detonation wave of each of these mechanisms? The mechanism of detonation remains unknown, despite numerous investigations over the past century (Fickett and Davis 1979; Fickett 1985). The major obstacle in determining reaction mechanisms from experiment lies in the short time and spatial scales over which detonation occurs and is complicated by the extreme pressure and energy releases accompanying the detonation.

Recent advances in spectroscopic methods are beginning to allow the direct measurements of molecular changes in a system that is shocked, toward the goal of determining the atomistic processes involved in the detonation (Gupta 1995). Others are investigating energy transfer rates (Fried and Ruggiero 1994) and mechanisms (Dlott and Fayer 1990; Tokmakoff, Fayer, and Dlott 1993; Chen, Tolbert, and Dlott 1994; Chen, Hong, Hill, and Dlott 1995) in energetic materials and possible relationships to the initiation of the detonation. These studies are providing critical pieces to a multifaceted chemical problem that is not completely understood. The measurements of molecular changes of explosives, however, have not been made under the extreme conditions associated with detonation. Direct measurement of chemical reactions occurring during this destructive and rapid event remains a formidable hurdle that has not been overcome.

As the development of diagnostic tools to measure these ultrafast events has progressed, computational resources and theoretical methods to model atomistic processes involved in the detonation have advanced as well. Early reactive models used in molecular dynamics simulations described molecular crystals consisting of diatomics in metastable bound states that, when shocked, dissociated exothermically to form the more stable monatomic products (Karo, Hardy, and Walker 1978; Tsai and Trevino 1981). A more recent study (Kawakatsu and Ueda 1988, 1989; Kawakatsu, Matsuda, and Ueda 1988), in which molecular dynamics simulations of the detonation were compared to hydrodynamic predictions, used an isomerization of the reactant as the energy-release reaction that drives the detonation. Although these models predicted reasonable pressure and temperature rises when compared to observed data from actual detonations, the chemistry that drives the detonation in these models is qualitatively unrealistic. A next step toward a more realistic description of the chemical processes occurring in a detonation would be one in which the energy

release is due to endothermic dissociation of the reactants followed by exothermic association of the fragments to form more stable products. One must proceed in this process slowly, that is, introducing a minimum of additional complexity in the reaction mechanisms so as not to mask incremental information which might result.

Brenner and coworkers (Brenner 1992; Robertson et al. 1992; White et al. 1992, 1994; Brenner et al. 1993), in attempts to describe more realistically exothermic chemical reactions occurring in a shock wave, developed a series of models based on gas-phase reactivity schemes. The models describe a heteronuclear diatomic molecular crystal that requires energy to break the molecular bonds in the low-pressure crystal, but releases substantial energy upon formation of homonuclear products. Two-dimensional molecular dynamics simulations using their first model (Brenner 1992; Robertson et al. 1992; White et al. 1992, 1994) (denoted Model 0 hereafter) appeared to sustain shock waves that were driven by exothermic reactions. However, the macroscopic property profiles (pressure, density, and temperature) of the detonating system were flat-topped and split (Brenner 1992; Robertson et al. 1992; White et al. 1992, 1994)—this behavior has not been observed in experiment. The results of a second study (Brenner et al. 1993) using a similar model (the only difference being in the molecular-size parameter) showed macroscopic shock profiles that agreed well with the simplest model of detonation (Fickett and Davis 1979; Fickett 1985), in which reaction takes place immediately behind the shock front. We will denote this model hereafter as Model I. Features of these models will be discussed below.

The studies described in this paper and an accompanying paper (Rice et al., in press) were partially prompted after our attempts to reproduce simulation results (published in Brenner et al. 1993) using Model I failed. Additionally, Model I (as well as Model 0) had features in the potential energy surface that seemed undesirable to us, as described later in this report. We made changes to Model I by removing these undesired features (the revised model denoted as Model II hereafter) and then performed two-dimensional molecular dynamics simulations of the detonation of this model energetic crystal initially at low temperature, low pressure. The equation of state and Hugoniot curve for this model were also obtained from two-dimensional molecular dynamics simulations at appropriate temperatures and pressures. These were used to make hydrodynamic predictions of detonation pressures, densities, and velocities. The hydrodynamic predictions were in good agreement with the results of our simulations of the detonation, indicating that our model and the method of molecular dynamics are consistent with the conservation laws of the process of detonation.

The focus of the study reported here is to examine the microscopic details of the detonation process and extract information concerning the mechanism of the detonation. We will first provide a detailed analysis of the interaction potentials for Models 0, I, and II and show that the reaction mechanisms of these systems, when subjected to shock, are strongly dependent on the functional form of the models. Then, using the results from two-dimensional molecular dynamics simulations reported in our accompanying paper (Rice et al., in press), we will dissect the reaction zone and follow the changes in molecular properties throughout this region. This will reveal the mechanism of detonation for this model.

2. MODELS

2.1 Models 0 and I. Models 0 and I, used by Brenner (Brenner 1992; Robertson et al. 1992; White et al. 1992; White et al. 1994; Brenner et al. 1993), are two-dimensional crystals of diatomic molecules arranged in a herringbone lattice. The interaction potential that is used to describe these crystals is

$$V = \sum_i^N \sum_{j>i}^N \left\{ f_c(r_{ij}) \left[V_R(r_{ij}) - \overline{B}_{ij} V_A(r_{ij}) \right] + V_{vdW}^{(1)}(r_{ij}) \right\}, \quad (1)$$

the sums being over the N atoms comprising the model. The functional forms and parameters for the terms in Equation (1) are given in Table 1. The expression in Equation (1) is based on ideas proposed and developed by Abell (1985) and Tersoff (1988). The left-most terms within the summations in Equation (1) make up the intramolecular interaction potential of diatomic molecules, and the second term within the sums, V_{vdW} , is an intermolecular interaction term. The function $f_c(r_{ij})$ smoothly attenuates the molecular-bonding interaction to zero at 3.0 Å. The bond-order function \overline{B}_{ij} , which ranges in value from zero to one depending on the local atomic environment, introduces many body effects by modifying the attractive term of the molecular-bonding portion of Equation (1), $V_A(r_{ij})$. For an isolated diatomic, the value of \overline{B}_{ij} is one, and $V_A(r_{ij})$ will have a maximum contribution to Equation (1) for the ij pair at the specified internuclear distance. If the diatomic is closely surrounded by many other atoms, as in the high-density region of a shock-compressed crystal, the value of \overline{B}_{ij} decreases, depending on the number and location of the nearest neighbors surrounding the ij pair. This decrease in \overline{B}_{ij} will correspondingly decrease the attractive interaction for the ij pair. This rubric is intended to mimic modifications of the bonding character upon increased density. As is made clear by the notation for the parameters given in

Table 1. Parameters and Functional Forms Used for the Potential Energy Expressions in Equations (1) and (2)

Parameter	Model 0 ^a	Model I ^b	Model II	Functional Form
$D_eAA(\text{eV})$	5.0	5.0	5.0	$V_R(r) = \frac{D_e}{S-1} \exp[-\alpha\sqrt{2S}(r-r_e)]$
$D_eBB(\text{eV})$	5.0	5.0	2.0	
$D_eAB(\text{eV})$	2.0	2.0	1.0	$V_A(r) = \frac{SD_e}{S-1} \exp\left[-\alpha\sqrt{\frac{2}{S}}(r-r_e)\right]$
$r_eAA(\text{\AA})$	1.0	1.2	1.2	
$r_eBB(\text{\AA})$	1.0	1.2	1.5	$\bar{B}_{ij} = \frac{1}{2}(B_{ij}+B_{ji})$
$r_eAB(\text{\AA})$	1.0	1.2	1.35	
S	1.8	1.8	1.8	$B_{ij} = \left\{ 1+G \sum_{k \neq i,j} f_c(r_{ik}) \exp[m(r_{ij}-r_{ik})] \right\}^{-n}$
$\alpha(\text{\AA}^{-1})$	2.7	2.7	2.7	
G	5.0	5.0	7.5	$\left\{ \begin{array}{l} 1, \\ 0, \end{array} \right. \quad \begin{array}{l} r < 2.0 \\ 2.0 \leq r < 3.0 \\ 3.0 \leq r \end{array}$
$m(\text{\AA}^{-1})$	2.25	2.25	3.5	$f_c(r_{ij}) = \left\{ \begin{array}{l} 1, \\ \frac{1}{2} [1 + \cos(\pi[r-2])], \\ 0, \end{array} \right. \quad \begin{array}{l} r < 2.0 \\ 2.0 \leq r < 3.0 \\ 3.0 \leq r \end{array}$
n	0.5	0.5	0.5	
$\epsilon(\text{eV})$	0.005	0.005	0.005	
$\sigma(\text{\AA})$	2.988	2.988	2.988	
$mass_A(\text{amu})$	14.0	14.0	15.0	
$mass_B(\text{amu})$	14.0	14.0	46.0	
$P_0(\text{eV})$	0.4727	0.4727	0.4854	$V_{vdW}^1 = \left\{ \begin{array}{l} 0, \\ P_0 + r[P_1 + r(P_2 + rP_3)] \\ 4e \left[\left(\frac{\sigma}{r} \right)^{12} - \left(\frac{\sigma}{r} \right)^6 \right] \\ 0 \end{array} \right. \quad \begin{array}{l} r < 1.75 \\ 1.75 \leq r < 2.91 \\ 2.91 \leq r < 7.32 \\ 7.32 \leq r \end{array}$
$P_1(\text{eV}\cdot\text{\AA}^{-1})$	-0.6996	-0.6996	-0.7184	
$P_2(\text{eV}\cdot\text{\AA}^{-2})$	0.3364	0.3364	0.3455	
$P_3(\text{eV}\cdot\text{\AA}^{-3})$	-0.0520	-0.0520	-0.05344	
$c_3(\text{eV}\cdot\text{\AA}^{-3})$			925.4631	
$c_4(\text{eV}\cdot\text{\AA}^{-4})$			138743.7872	
$c_5(\text{eV}\cdot\text{\AA}^{-5})$			5548241.6326	$V_{vdW}^2 = \left\{ \begin{array}{l} 0, \\ P_0 + r[P_1 + r(P_2 + rP_3)] \\ 4e \left[\left(\frac{\sigma}{r} \right)^{12} - \left(\frac{\sigma}{r} \right)^6 \right] \\ \sum_{i=3}^5 c_i(r-7.32)^i \\ 0 \end{array} \right. \quad \begin{array}{l} r < 1.75 \\ 1.75 \leq r < 2.91 \\ 2.91 \leq r < 7.31 \\ 7.31 \leq r \leq 7.32 \\ 7.32 \leq r \end{array}$

^aReference Brenner (1992). There is a typographical error in Table 1 of this reference for the B_{ij} definition (Brenner, private communication). It is corrected in Brenner et al. (1993).

^bBrenner et al. (1993).

Table 1, this form of the potential is capable of describing diatomic molecules formed by atoms of types A-B, A-A, and B-B as well as intermolecular interactions between these various atom types. The curves in Figure 1(a) illustrate the effect of the $\overline{B_{ij}}$ term on the intramolecular term for an A-B pair. The 11 curves in this figure correspond to the A-B intramolecular interaction with $\overline{B_{ij}}$ values ranging from 0 to 1. This figure shows that the ij attraction is decreased by over one-half for $\overline{B_{ij}} = 0.7$, and the molecular interaction appears to be completely repulsive for $\overline{B_{ij}} < 0.1$. Also, the positions of the potential energy minima increase with decreasing $\overline{B_{ij}}$. The behavior of this function with decreasing $\overline{B_{ij}}$ indicates that as the local atomic environment becomes increasingly dense around an ij pair, the i and j atoms will be "forced apart" by the increased repulsion that can be attributed to this functional form.

Figure 1(b) shows the effect of the $\overline{B_{ij}}$ term on the intramolecular term for an A-A (or B-B) pair. (The masses and homonuclear interactions of A and B atoms are the same in Model 0). As in Figure 1(a), the intramolecular attraction is decreased by over one-half for $\overline{B_{ij}} = 0.7$ and becomes completely repulsive for $\overline{B_{ij}} < 0.1$. However, due to the differences in well depths for the intramolecular potential for A-A (or B-B) pairs and the A-B pairs, the attractive interactions for A-A pairs are considerably greater than A-B pairs for most values of $\overline{B_{ij}}$.

Brenner and coworkers found that Model 0 produced "flat-topped, split shock-wave structure" of the detonating crystal that is due to a "high-pressure, dissociative phase transition unintentionally introduced through our initial parameterizations" (Brenner 1993). In our preliminary studies using Model 0, we were able to reproduce each feature of the potential energy surface that was reported (Brenner 1992; Robertson et al. 1992; White et al. 1992; White et al. 1994), including sound speed, equilibrium nearest-neighbor distance, barrier to collinear reaction of A + A-B, and shock wave velocities. We also reproduced the flat-topped split shock-wave structures alluded to in footnote 13 of Brenner (1993).

Brenner et al. subsequently published results from simulations using Model I in which the "high-pressure, dissociative phase transition" does not occur, and the detonation profiles show a single shock front that is followed by a reacting flow and rarefaction wave (Brenner 1993). The results using Model I were those that we could not reproduce.

Model I, as reported in Brenner (1993), is the same as Model 0 with one difference; that is, the value of r_e . In Model 0, r_e had a value of 1.0 Å; r_e in Model I is 1.2 Å. Thus, the changes in intramolecular

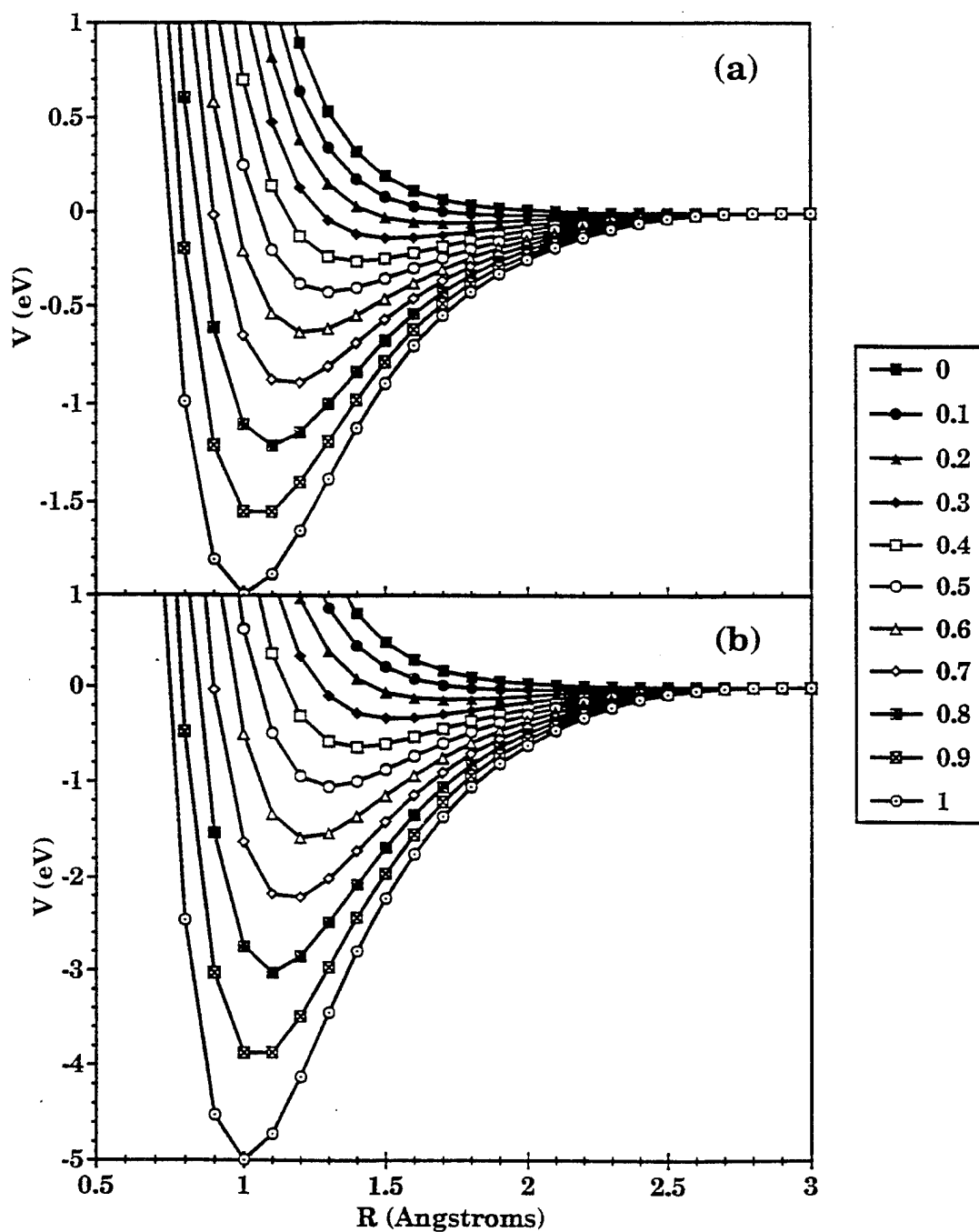


Figure 1. Intramolecular interaction potentials of Model 0 for different B_{ij} values (Equation 1) as functions of internuclear distance for (a) A-B interactions; (b) A-A interactions. Magnitude of the B_{ij} values are denoted in the legend.

interaction potential with \overline{B}_{ij} for Model I are similar to those of Model 0, shown in Figure 1, with the equilibrium distances shifted by 0.2 Å for each curve.

Using the parameters of Model I, we have performed molecular dynamics simulations in an attempt to reproduce results of Brenner (1993). However, we once again saw the flat-topped, split shock-wave structure that was seen in Model 0. Figure 2 is a snapshot of the detonating system at 15 ps resulting from our simulations using Model I. This snapshot shows that four distinct regions exist: the undisturbed crystal, a compressed crystal in which the molecules are reoriented, but do not react; the "high-pressure, dissociative phase transition" (Brenner 1993) in which molecular identity is lost, and the rarefaction region, consisting of vibrationally excited homonuclear products. The velocities of the two leading discontinuities are 8.1 and 6.8 km/s, respectively, whereas Brenner (1993) reported the velocity of the single shock front as 9.3 km/s.

We do not know the source of the discrepancies between our calculations and those of Brenner (1993). Several details about the calculations, particularly regarding the initial conditions, were not given in Brenner (1993), including the equilibrium molecular orientation, lattice constants, temperature of the undisturbed crystal, and number of atoms in the system. We therefore had to attempt to reproduce the simulations reported in Brenner (1993) with an incomplete set of information. We determined the equilibrium low-pressure (1 atm), low temperature (20 K) crystal structure for Models 0 and I using NPT Metropolis Monte Carlo sampling as described in Rice et al. (in press). The low-temperature, ambient-pressure lattice parameters of the crystal defined by Model I in the x- and y directions are $a = 4.16$ Å and $b = 6.25$ Å, respectively. The center-of-bond (COB) fractionals for the two molecules (1 and 2) in the unit cell are at (0.25, 0.25) and (0.75, 0.75), respectively. The equilibrium A-B bond length is 1.19945 Å, and the molecular orientation of molecules 1 and 2 are 30.51° and -30.51° , respectively, relative to the crystal x-axis. The details of the molecular dynamics simulations are given in Section 3.4 of Rice et al. (in press).

Upon finding these discrepancies in our calculations when compared to those published in Brenner (1993), we attempted to understand the source of the "dissociative phase transition," which seemed to cause the problem of the flat-topped shock structure. We began our analyses by examining the three-body molecular interaction term that includes \overline{B}_{ij} for Model I. We generated contour plots, shown in Figure 3 of the collinear reactions:

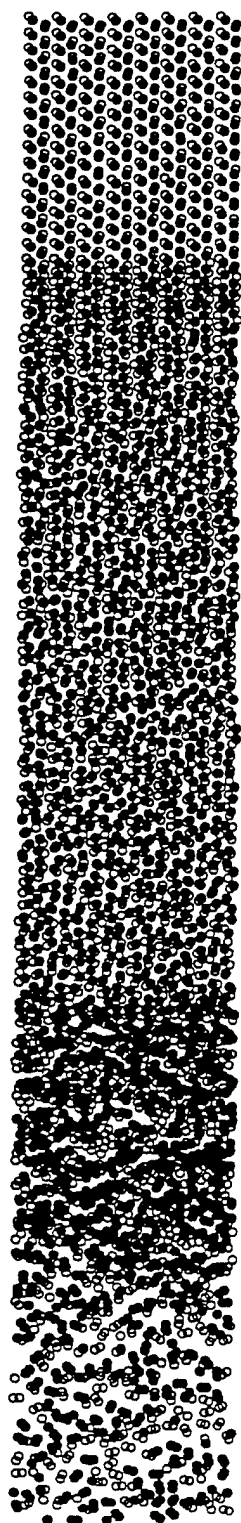


Figure 2. Snapshot of chemically sustained shock waves at 15 ps initiated by a four-layer flyer plate with an impact velocity of 6 km/s. The model used in this simulation is Model I (Brenner et al. 1993). The two types of atoms are depicted by filled and empty circles. Dimensions of the portion of the crystal shown in this snapshot are 387 by 50 Å.

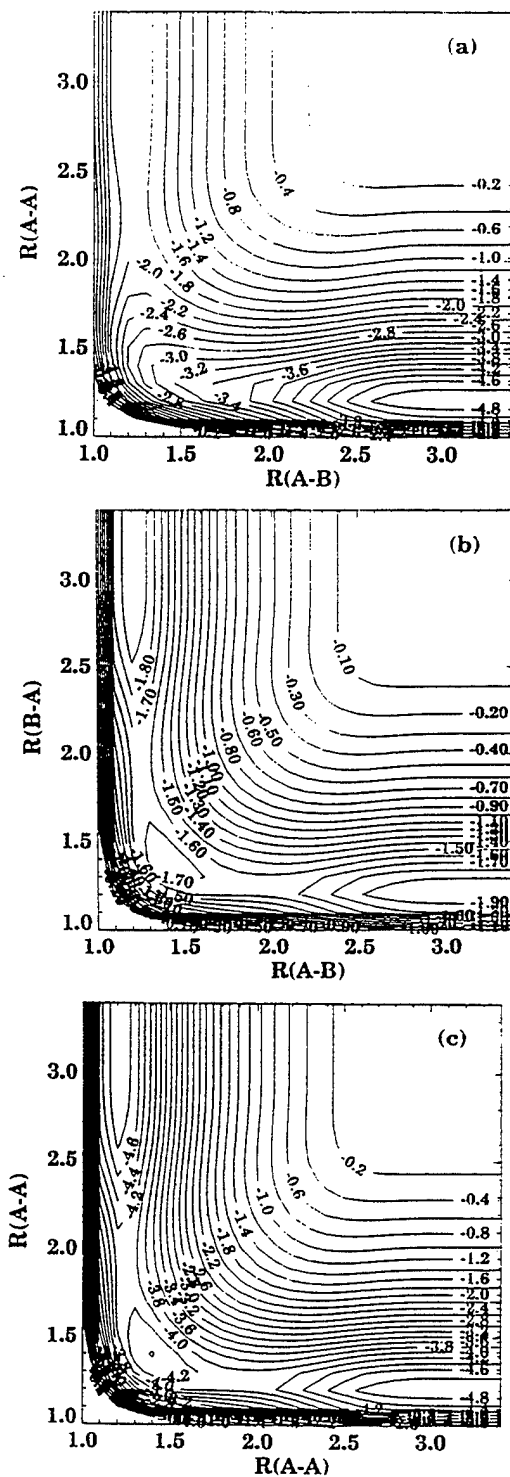


Figure 3. Potential energy contours (in eV) for the following collinear three-body reactions using Model I: (a) $A + A-B \rightarrow A-A + B$; (b) $A + BA \rightarrow A-B + A$; (c) $A + A-A \rightarrow A-A + A$. Units for the internuclear distances along both axes are in Å.



Note that because the masses and bond energies of A-A and B-B are the same for Model I, that reactions (I)–(III) have the same potential energy features as the following collinear reactions:



As previously stated, we were able to reproduce the contour plot and barrier to Reaction (I) for Model 0, given in Brenner (1992), Robertson et al. (1992), and White et al. (1992, 1994). Figure 3(a), the contour of Reaction (I) for Model I, is similar in feature to the contour of Model 0 given in Brenner (1992), Robertson et al. (1992), and White et al. (1992, 1994); we calculate a barrier to reaction upon collinear approach as 0.10 eV, whereas the value reported in Brenner (1993) is 0.08 eV (this may not be significant).

However, as is evident in Figures 3(b) and 3(c), the trimers ABA and AAA exist upon linear approach. (Due to the features of the potential, this indicates that the trimers BAB and BBB also exist.) We characterized these species through normal mode analyses, after finding the equilibrium structures of these trimers using the Newton-Raphson energy minimization method (Margenau and Murphy 1943). The geometries and vibrational frequencies of these species are given in Table 2. Also, we characterized the structures corresponding to the saddle points apparent in these figures. We were able to reproduce the features of the A-A and A-B diatomics that were reported in Brenner (1993), as well as the crystalline binding energy of 0.04 eV per molecule and nearest-neighbor distances of 3.3 Å. We were unable to locate any nonlinear trimers AAA or ABA or any of the trimers AAB or BBA using Equation (1) for either Models 0 or I. Higher order multimers were not found.

The relative energy features of the potential energy surface for Model I are illustrated in Figure 4. These schematics show relative energies of the trimers and the saddle points leading to their formation/decomposition. The shallow minima of the trimers relative to the saddle points leading to dissociation suggest that the trimers would be short-lived in a high-energy environment such as that which

Table 2. Geometric Parameters and Harmonic Vibrational Frequencies of Critical Points on the Potential Energy Surfaces for Models 0, I, and II

Species	Internuclear Distances (Å)	Harmonic Frequencies (cm ⁻¹)	Energy (eV)
Model 0			
A-B	R(A-B) = 1.00000	1064	-2.0
A-A (B-B)	R(A-A) = 1.00000	1682	-5.0
A-A-A (B-B-B)	R(A-A) = 1.24082	200, 296, 739	-3.94069
A-B-A (B-A-B)	R(A-B) = 1.23822	150, 184, 466	-1.58114
A + A-B -->A-A + B	R(A-A) = 2.15000 R(A-B) = 1.01298	217i, 982	-1.89457
A + B-A -->A-B-A	R(A-B) = 1.37625 R(B-A) = 1.14901	158i, 171, 570	-1.57884
A + A-A -->A-A-A	R(A-A) = 1.35566 R(A-A) = 1.16141	225i, 280, 866	-3.93764
Model I			
A-B	R(A-B) = 1.2	1064	-2.0
A-A (B-B)	R(A-A) = 1.2	1683	-5.0
A-A-A (B-B-B)	R(A-A) = 1.38609	195, 690, 863	-4.42361
A-B-A (B-A-B)	R(A-B) = 1.38554	122, 439, 545	-1.77019
A + A-B -->A-A + B	R(A-A) = 2.28375 R(A-B) = 1.21310	257i, 974	-1.90225
A + B-A -->A-B-A	R(A-B) = 1.87013 R(B-A) = 1.24572	230i, 847	-1.64694
A + A-A -->A-A-A	R(A-A) = 1.87013 R(A-A) = 1.24572	365i, 1339	-4.11734
Model II			
A-B	R(A-B) = 1.35	727	-1.0
A-A	R(A-A) = 1.2	1626	-5.0
B-B	R(B-B) = 1.5	587	-2.0
A + B-A -->A-B + A	R(A-B) = 1.64967	300i, 275	-0.57237
B + A-B -->B-A + B	R(A-B) = 1.64967	171i, 157	-0.57237
A-B + B -->A + B-B	R(A-B) = 1.68460 R(B-B) = 1.79843	367i, 365	-0.82174
B + B-B -->B-B + B	R(B-B) = 1.79967	242i, 222	-1.14474
A + A-A -->A-A + A	R(A-A) = 1.49969	670i, 631	-2.86186

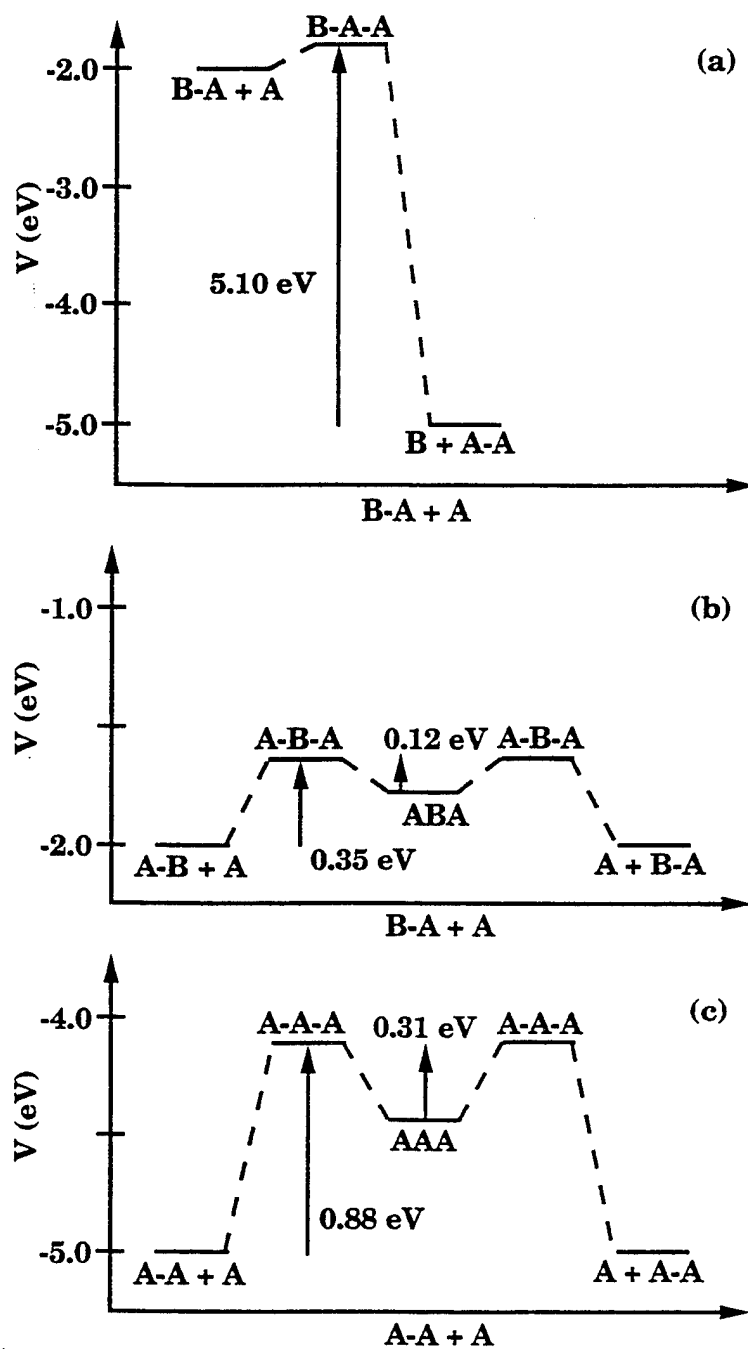


Figure 4. Schematic of the potential energy for three-body collinear reactions (I)–(III) for Model I.

exists behind the shock front. Additionally, the trimer minima will be affected by the density, since trimer existence is due to the intramolecular interaction term in Equation (1). The effect on the trimer minima due to the changes in density as the shock front travels through the region will affect the lifetime of the trimer intermediate. The ability of Equation (1) to form trimers leads us to suspect this might explain the region in the detonating system that Brenner et al. call the "dissociative phase-transition" (Brenner 1993). We think it might be more appropriate to label that region as an *associative* phase-transition, where trimer formation occurs, leading to subsequent decomposition to the more stable homonuclear diatomic species. In any case, changing the value of the parameter r_e from 1.0 to 1.2 Å did not remove the source of the "flat-topped, split shock-wave structure" (Brenner 1993), which we think is due to this ability to form trimers.

2.2 Model II. The ability of trimer formation using Models 0 and I indicated to us that saturation of the molecular bond was not correctly accounted for in Equation (1) with those sets of parameters. It seems appropriate to us that not only should the attractive portion of the potential be modified according to the local atomic environment, but that the repulsive wall should be affected as well, to take into account saturation of the bonds. We have therefore modified Equation (1) to

$$V = \sum_i^N \sum_{j>i}^N \left\{ f_c(r_{ij}) \left[(2 - \overline{B}_{ij}) V_R(r_{ij}) - \overline{B}_{ij} V_A(r_{ij}) \right] + V_{vdW}^{(2)} \right\}, \quad (2)$$

where the term \overline{B}_{ij} has the same description as in Equation (1). The parameters and functional form for the terms in Equation (2) are given in Table 1. We found two discontinuities in the weak long-range van der Waals interaction for Models 0 and I; one at $r = 2.91$ Å and the other at $r = 7.32$ Å. We have corrected the discontinuity at $r = 2.91$ Å by determining the cubic spline coefficients using the requirements that at $r = 1.75$ Å, the energy and energy first derivatives must equal 0.0, and at $r = 2.91$ Å, the energy and energy first derivatives must equal that produced by the Lennard-Jones potential function. We also added a quintic spline to the Lennard-Jones potential in the region of 7.31–7.32 Å, to allow a continuous cutoff of the intermolecular interaction. The quintic spline coefficients were determined in the same manner as the cubic spline coefficients described earlier; however, energy second derivatives were required to match at the functional interfaces at 7.31 Å and 7.32 Å. We have only provided four significant figures for the spline coefficients used in Equation (2); we suggest that machine accuracy of these coefficients be determined by the interested modeler.

We have also changed the model parameters to allow different exothermic reactions, and set the masses of particles A and B to 15 and 46 amu, respectively, in order to introduce mass effects. Also, the molecular sizes of the A-B, A-A, and B-B diatomics were set to 1.35, 1.2, and 1.5 Å, respectively. The reactions that this model describes are:



Geometric parameters and vibrational frequencies of the stable species for these reactions are given in Table 2. We also show contour plots of the collinear reactions using Equation (2), assuming only three atoms, in Figure 5. We did not find trimer or other multimer formations using Equation (2). For the collinear approach of A to A-B, there is no barrier to approach. The transition state structures and vibrational frequencies for the collinear reactions are also given in Table 2.

We have given considerable attention to describing the features of the potential energy surface for Model II assuming only three atoms, primarily because such attention was given in the previous studies for Models 0 and I (Brenner 1992; Robertson et al. 1992; White et al. 1992, 1994; Brenner 1993) and we wished to provide direct comparison. However, in the high-dense region behind the shock wave, the potential energy interactions (specifically the intramolecular interactions) will be affected by many more atoms than three. Therefore, as we did for Model 0, we show the effect of the intramolecular interaction with different values of $\overline{B_{ij}}$ in Figure 6, which correspond to varying degrees of density of atoms surrounding an ij pair.

These curves differ from those of Model 0 (Figure 1) in that the well depths are decreased by one-half for $\overline{B_{ij}} = 0.8$ rather than $\overline{B_{ij}} = 0.7$. Additionally, the repulsive interactions for these $\overline{B_{ij}}$ values are much greater than those for Model 0, and the positions of the minima are at larger distances with decreasing $\overline{B_{ij}}$ than those for Model 0. This model is analogous to Models 0 and I in that the atoms are forced apart with decreasing $\overline{B_{ij}}$.

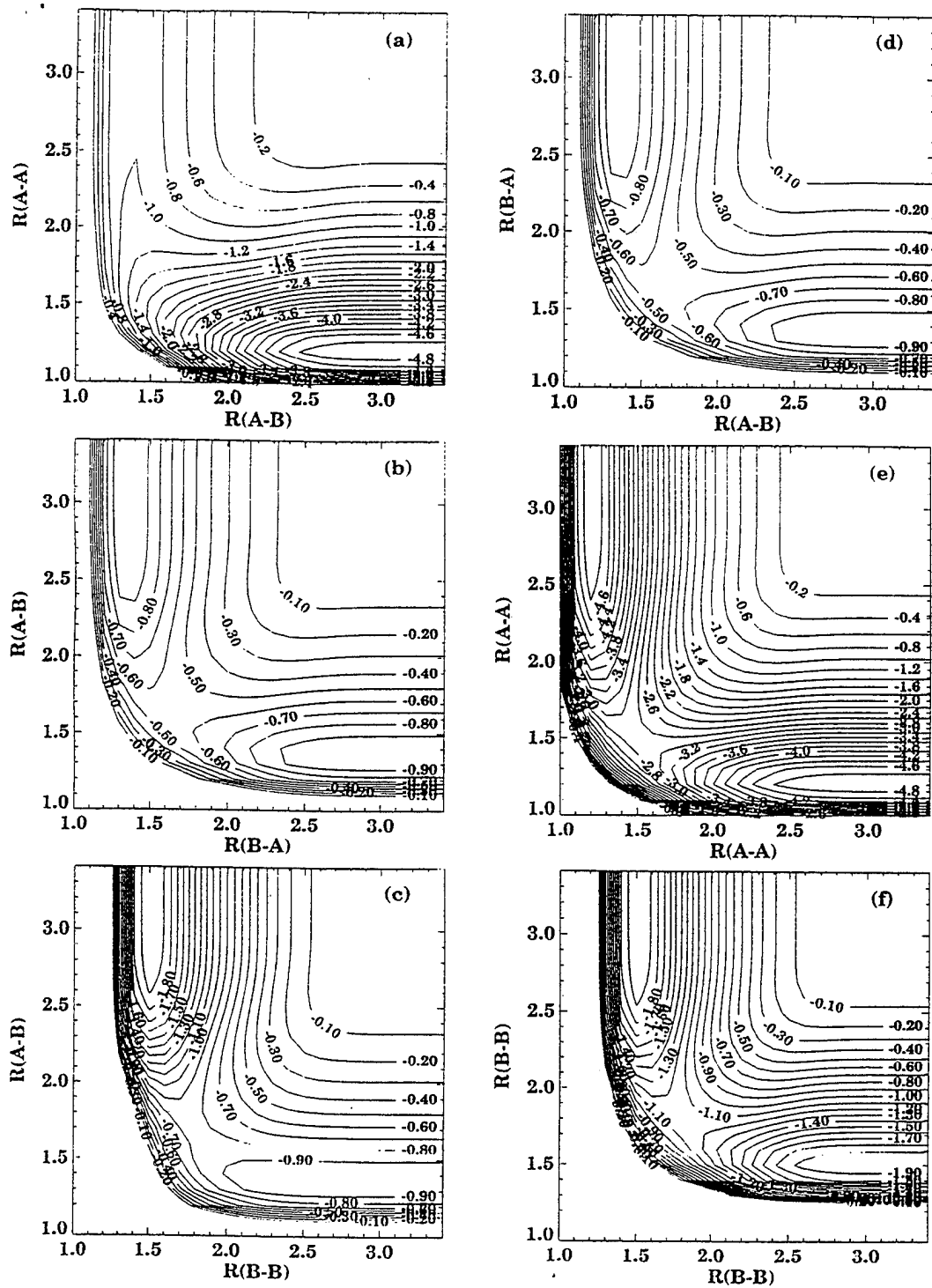


Figure 5. Potential energy contours (in eV) for the following collinear three-body reactions using Model II: (a) $A + A-B \rightarrow A-A + B$; (b) $A + B-A \rightarrow A-B + A$; (c) $A + B-B \rightarrow A-B + B$; (d) $B + A-B \rightarrow B-A + B$; (e) $A + A-A \rightarrow A-A + A$; (f) $B + B-B \rightarrow B-B + B$. Units for the internuclear distances along both axes are in Å.

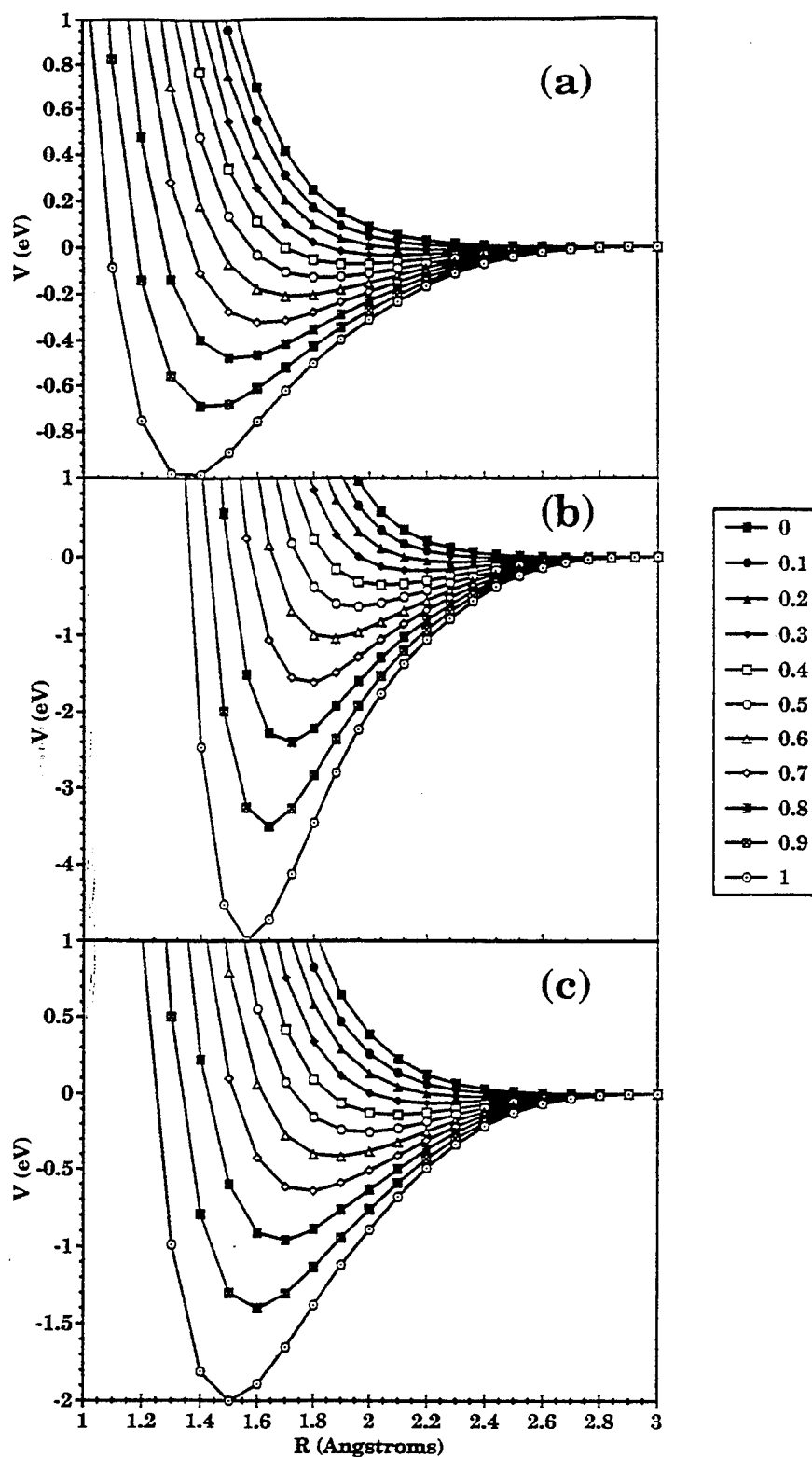


Figure 6. Intramolecular interaction potentials of Model II for different $\overline{B_{ij}}$ values (Equation 2) as functions of internuclear distance for (a) A-B interactions; (b) A-A interactions; and (c) B-B interactions. Magnitude of the $\overline{B_{ij}}$ values are denoted in the legend.

The two-dimensional crystal modeled by Equation (2) also has an equilibrium configuration consistent with a herringbone arrangement. We determined the 1 atm, 20 K orientation of the crystal using the NPT Monte Carlo calculations (described in Rice et al., in press). The low-temperature, ambient-pressure lattice parameters of the crystal in the x and y directions, respectively, are $a = 4.34 \text{ \AA}$, $b = 6.27 \text{ \AA}$. The COB fractionals for the two molecules (1 and 2) in the unit cell are at 0.25, 0.25 and 0.75, 0.75, respectively. The A-B equilibrium bond length is 1.349 \AA , and the molecular orientation of molecules 1 and 2 are 29.0° and -29.0° , respectively, relative to the crystal x-axis.

NPT Metropolis Monte Carlo calculations of equilibrium crystal structure as a function of pressure at 20 K were performed to determine the sound speeds of the different models. Results of the density as a function of pressure for Models I and II are shown in Table 3. These results for P ranging from 0.0 to 0.015 eV/\AA^2 were fitted to a cubic polynomial, and the slope of P-V curve was extracted, which is directly proportional to the square of the sound speed of the crystal (Fickett and Davis 1979; Fickett 1984). The sound speeds for Models I and II are 2.0 and 1.2 km/s, respectively.

3. DETAILS OF THE CALCULATIONS

Details of the molecular dynamics simulations are given in the accompanying paper on the comparison of molecular dynamics simulations to hydrodynamic predictions (Rice et al., in press). The results that are analyzed in this paper are from the simulation in which shock is initiated by a plate of A-A molecules striking the simulation cell with an impact velocity of 12 km/s.

Because our interest is to examine the mechanistic details involved in the reactions initiating the detonation, we will focus our analysis on a region we call the reaction zone. The reaction zone here is defined as the region between the shock front and the point at which the number of reacted A-B molecules equals or exceeds the number of unreacted A-B molecules. It is difficult to determine whether a molecule has reacted or not within this zone in an unambiguous manner, due to the effect on Equation (2) by the higher density of this region. As shown earlier, there exists a density of nuclei [reflected by the $\overline{B_{ij}}$ term of Equation (2)] that eliminates any attraction between the A-B pair, even though the atoms are within the 3.0 \AA cutoff for the intramolecular term. However, we know unambiguously that some sort of molecular interaction exists if the A-B internuclear distance is less than 3.0 \AA according to Equation (2). Therefore, for simplicity, we have used the following simple geometric test to determine reactivity. We have defined that the original A-B pair has undergone reaction (is dissociated, or is bound to an atom that

Table 3. Lattice Parameters, Density, and Molecular Geometries vs. Pressure for Models I and II

Pressure (eV/Å ²)	Model I					Model II				
	<a> (Å)	 (Å)	<ρ> (amu/Å ²)	<r _{ij} > (Å)	<θ _{ij} > (deg)	<a> (Å)	 (Å)	<ρ> (amu/Å ²)	<r _{ij} > (Å)	<θ _{ij} > (deg)
0.0	4.16	6.25	2.1538	1.200	30.3	4.34	6.27	4.4833	1.349	29.1
0.00005	4.17	6.23	2.1556	1.199	29.7	4.33	6.28	4.4865	1.349	29.3
0.0001	4.16	6.24	2.1573	1.199	30.0	4.33	6.27	4.4937	1.349	29.1
0.0005						4.32	6.25	4.5185	1.349	29.1
0.001	4.16	6.18	2.1782	1.199	29.2	4.31	6.22	4.5508	1.349	29.0
0.0025						4.24	6.19	4.6484	1.349	29.8
0.005	4.10	6.03	2.2651	1.199	28.7					
0.01	4.04	5.94	2.3336	1.198	28.9					
0.0125						4.13	5.94	4.9731	1.347	29.0
0.015						4.11	5.90	5.0311	1.346	29.0

is not its original molecular partner) if the distance between the atomic centers exceeds 3.0 Å. Figure 8(d) of Rice et al. (in press) shows the number of unreacted A-B molecules and dissociated A-B molecules at 7.8 ps in the simulation. The point at which the number of dissociated A-B molecules exceeds the number of unreacted A-B molecules falls slightly behind the shock fronts in the density, pressure, and temperature profiles. As shown in Rice et al. (in press), the width of the reaction zone is approximately constant throughout the simulations of unsupported detonations and is, on average, 14 Å wide.

We will examine the translational, rotational, and vibrational kinetic energy (KE) distributions of all unreacted A-B molecules within the reaction zone. Before the KE components for each molecule are calculated, the local mass flow velocity is removed as described in Rice et al. (in press). Additionally, we will calculate the distributions of A-B bond lengths and orientation angles of the A-B molecules relative to the crystal x-axis in this region. We will also calculate the distributions of the intramolecular interaction potential and the $\overline{B_{ij}}$ term for the unreacted A-B molecules. The calculation of the translational energy of the unreacted A-B molecule is straightforward:

$$\text{KE (Translation)} = \frac{P_{\text{CM}}^2}{2M}, \quad (3)$$

where M is the total mass of the A-B molecule and P_{CM} is the center-of-mass momentum of the molecule. As an approximation, we assume that the rotational energy is the KE due to motion of the atoms in the molecule that are perpendicular to the molecular bond

$$\text{KE (Rotation)} = \frac{1}{2} \sum_{i=A}^B m_i v_{i(\text{perpendicular})}^2, \quad (4)$$

where $v_{i(\text{perpendicular})}$ denotes the velocity components perpendicular to the molecular bond (center-of-mass velocity removed). The vibrational KE is the KE due to motion of the atoms in the molecule along the molecular bond

$$\text{KE (Vibration)} = \frac{1}{2} \sum_{i=A}^B m_i v_{i(\text{parallel})}^2, \quad (5)$$

where $v_{i(\text{parallel})}$ denotes the velocity components parallel to the molecular bond (center-of-mass velocity removed).

Although these calculations of the internal energy distributions are based on a simple idea, especially in light of the fact that the molecules might not even be bound in this zone due to the high-density effects on the interaction potential, it represents adequately energy flow into the directional components of the system.

4. RESULTS

Each of the calculations that simulated unsupported detonations discussed in Rice et al. (in press) (flyer-plate impact velocities ≥ 4.7 km/s) provide the same temperature, density, and pressure profiles as well as the same microscopic behavior in the reaction zone once the detonation wave reaches the steady-state velocity. Therefore, we are presenting the results of only one simulation, the simulation with plate impact of 12 km/s.

We have examined in detail the various properties within the reaction zone in order to detect any variations occurring there. The reaction zone is partitioned into seven regions, labeled 0-6. Each region has a 2.17 Å width in the crystal x direction (1/2 the size of the unit cell in the x direction), and because the shock profile is uniform in the y direction, the length in the y-direction is the entire crystal length. Region 0 is the area directly behind the shock front to 2.17 Å behind the shock front; region 1 begins at the end of region 0, and ends at 4.34 Å behind the shock front; region 2 ends 6.51 Å behind the shock front; and so on, concluding with region 6, which ranges from 13.02 to 15.19 Å behind the shock front. Distributions of properties of the system were calculated at every 100th integration step throughout the 12 km/s trajectory; cumulative distributions of these properties were compiled, normalized, and analyzed. The normalization is such that the integral of the property over the independent variable is one. Within the statistical uncertainty resulting from this limited sampling, none of the properties changed in time after the first 0.25 ps following flyer-plate impact. In order to obtain better statistical sampling, we therefore report cumulative normalized distributions and corresponding time averages for all times later than 0.5 ps after flyer-plate impact. We have calculated energy and orientational distributions of the unreacted A-B molecule that are in each region. Additionally, we have calculated the distributions of the intramolecular interactions and corresponding $\overline{B_{ij}}$ terms for the unreacted A-B pairs in these regions. Averages obtained

from the normalized distributions of these properties for each of the seven regions within the reaction zone are shown in Table 4.

Figures 7–9 show the cumulative translational, rotational, and vibrational KE distributions, respectively, of the unreacted A-B pairs in the seven zones throughout the 12 km/s simulation. It is evident that the translational modes of the A-B molecules in the region directly behind the shock front (region 0) are substantially excited as the shock wave passes through it, but the internal modes are excited to only one-quarter of the value of the translational excitation. The average translational energy of molecules within region 1 is less than half that of region 0, while the average energy of the internal modes has doubled, indicating that substantial energy transfer among molecular modes has occurred by the time the molecules have moved from region 0 to region 1. Since the average residence time of the molecules in each 2.17 Å region in the reaction zone is only 3.3×10^{-14} s (assuming local mass flow velocity of 6.6 km/s, the speed of the detonation wave in this simulation [Rice et al., in press]), energy transfer among molecular modes is rapid. Beyond region 1, the regional averages reach plateau values, consistent with equipartitioning of energy among translational and internal modes. It is evident that substantial vibrational excitation does not occur due to shock impact. Therefore, the mechanism of vibrational excitation to dissociation of A-B molecules from shock impact (thermal decomposition) is not consistent with this model.

Figures 10 and 11 show the distributions of molecular bonding energies for atom pairs and the $\overline{B_{ij}}$ terms within the seven regions. Figures 12 and 13 show the distributions of the internuclear A-B distances and rotational orientations within the seven regions. The distribution of the $\overline{B_{ij}}$ values in region 0 is spread across the range of values, reflecting high density behind the shock front, but has a broad maximum at 0.9. The average $\overline{B_{ij}}$ value for region 0 is 0.7. Figure 6 shows that the maximum A-B intramolecular attraction corresponding to this $\overline{B_{ij}}$ value is -0.3 eV when $R_{AB} = 1.6$ Å. The corresponding distribution for internuclear distances of the A-B molecules within region 0 (Figure 12), however, is a narrow distribution centered at 1.35 Å. A-B molecules with this internuclear distance and a $\overline{B_{ij}}$ value of 0.7 (or less) experience no attraction and different degrees of repulsion, depending on the actual $\overline{B_{ij}}$ value. This is reflected in the intramolecular potential energy distribution for the A-B pairs shown in Figure 10. The distribution has a peak at $V_{ij} = 0$ eV for region 0, but also has a shoulder extending from $V = 0$ to $V = -1$. The shoulder is due to the significant number of A-B molecules that

Table 4. Averages of Properties of Unreacted A-B Molecules in Reaction Zone
Throughout 12 km/s Simulation of Unsupported Detonation

Region	$\langle E(\text{Trans}) \rangle$ (eV)	$\langle E(\text{Rot}) \rangle$ (eV)	$\langle E(\text{Vib}) \rangle$ (eV)	$\langle V_{ij} \rangle$ (eV)	$\langle \bar{B}_{ij} \rangle$	$\langle r_{ij} \rangle$ (Å)	$\langle \theta_{ij} \rangle$ (deg)
0	1.1745	0.1336	0.1512	-0.3302	0.6767	1.4462	40.3
1	0.5027	0.2492	0.2821	0.0245	0.3070	1.8209	51.4
2	0.4077	0.2601	0.2472	0.0564	0.1622	2.0568	49.4
3	0.4334	0.2368	0.2387	0.0572	0.1553	2.0920	46.9
4	0.4578	0.2347	0.2420	0.0470	0.1425	2.1322	45.1
5	0.4608	0.2298	0.2289	0.0430	0.1411	2.1540	45.1
6	0.4805	0.2235	0.2208	0.0387	0.1413	2.1625	46.0

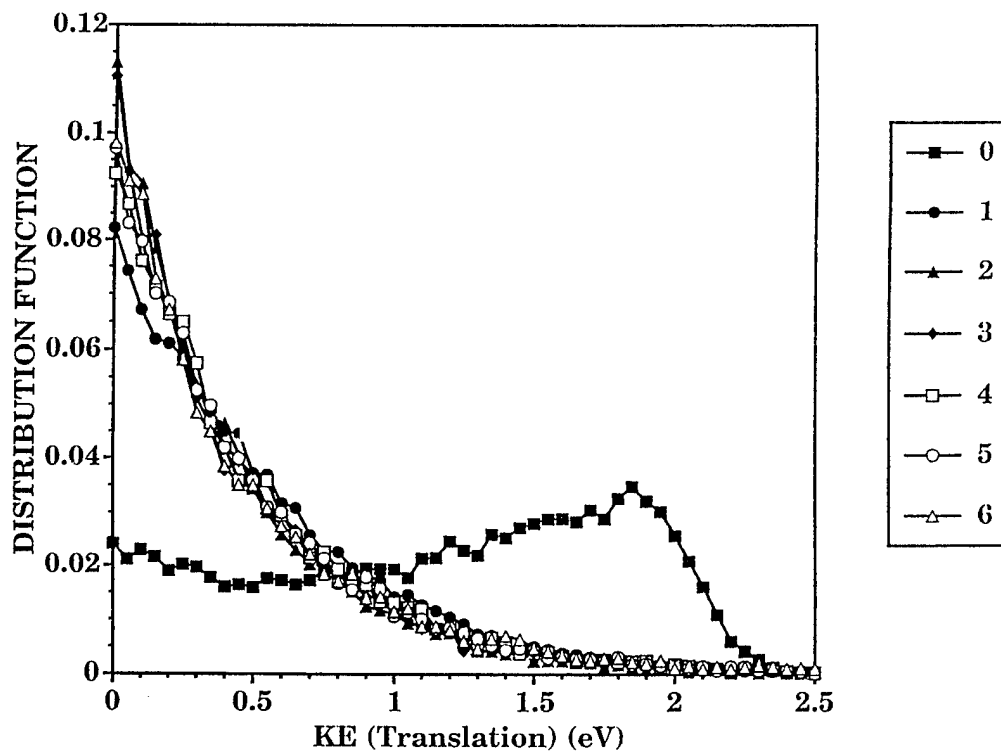


Figure 7. Normalized translational energy distributions of original A-B pairs for seven regions directly behind the shock front through the 12 km/s simulation (up to 7.8 ps). See text for definition of regions.

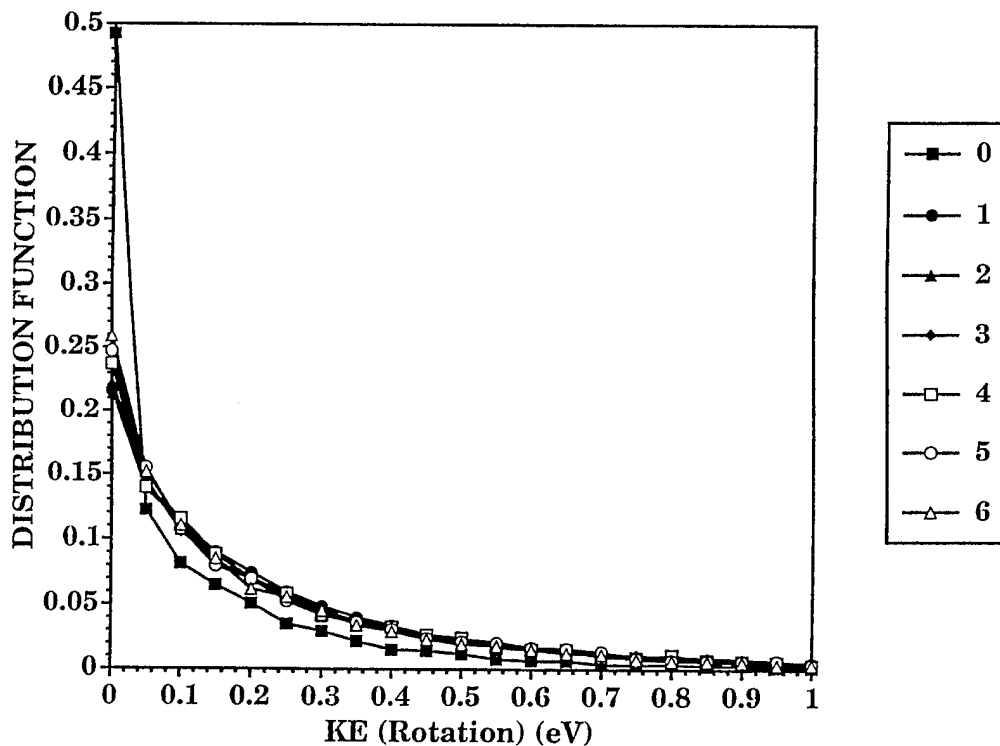


Figure 8. Normalized rotational energy distributions of original A-B pairs for seven regions directly behind the shock front through the 12 km/s simulation (up to 7.8 ps). See text for definition of regions.

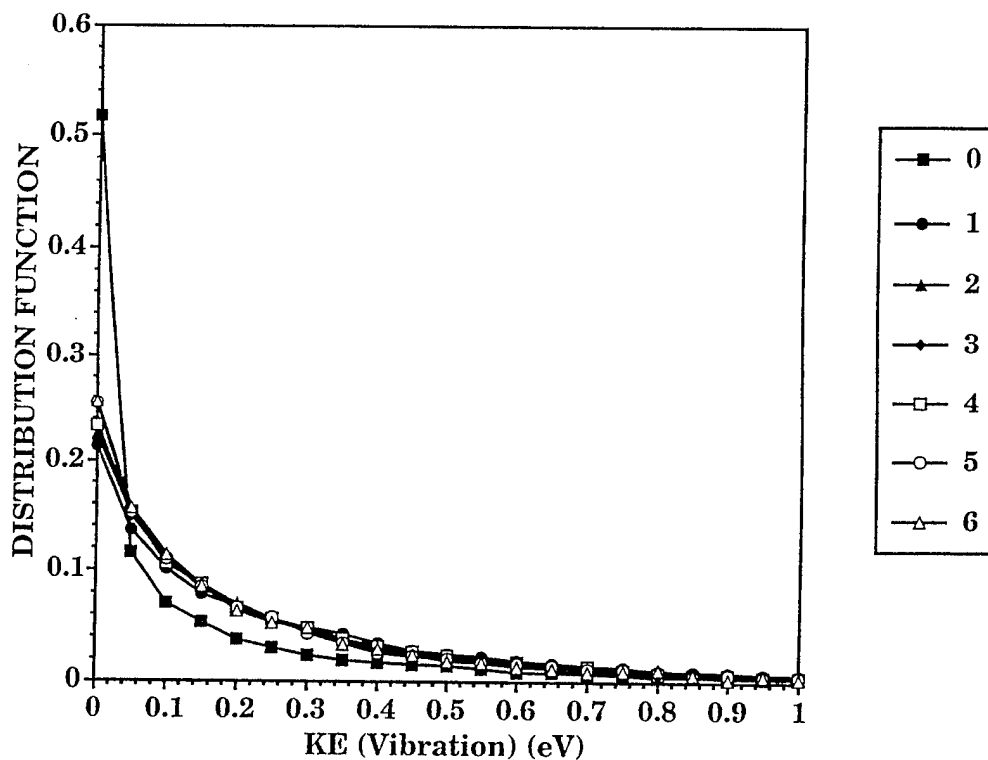


Figure 9. Normalized vibrational KE distributions of original A-B pairs for seven regions directly behind the shock front through the 12 km/s simulation (up to 7.8 ps). See text for definition of regions.

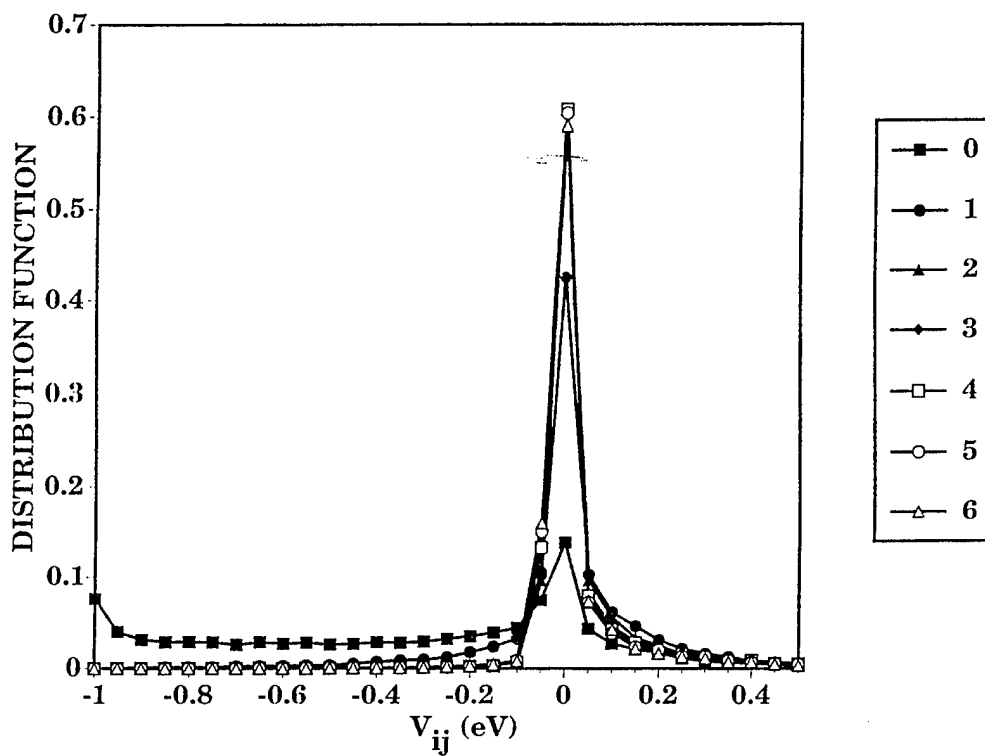


Figure 10. Normalized distribution of intramolecular terms of Equation (2) of original A-B pairs for seven regions directly behind the shock front through the 12 km/s simulation (up to 7.8 ps). See text for definition of regions.

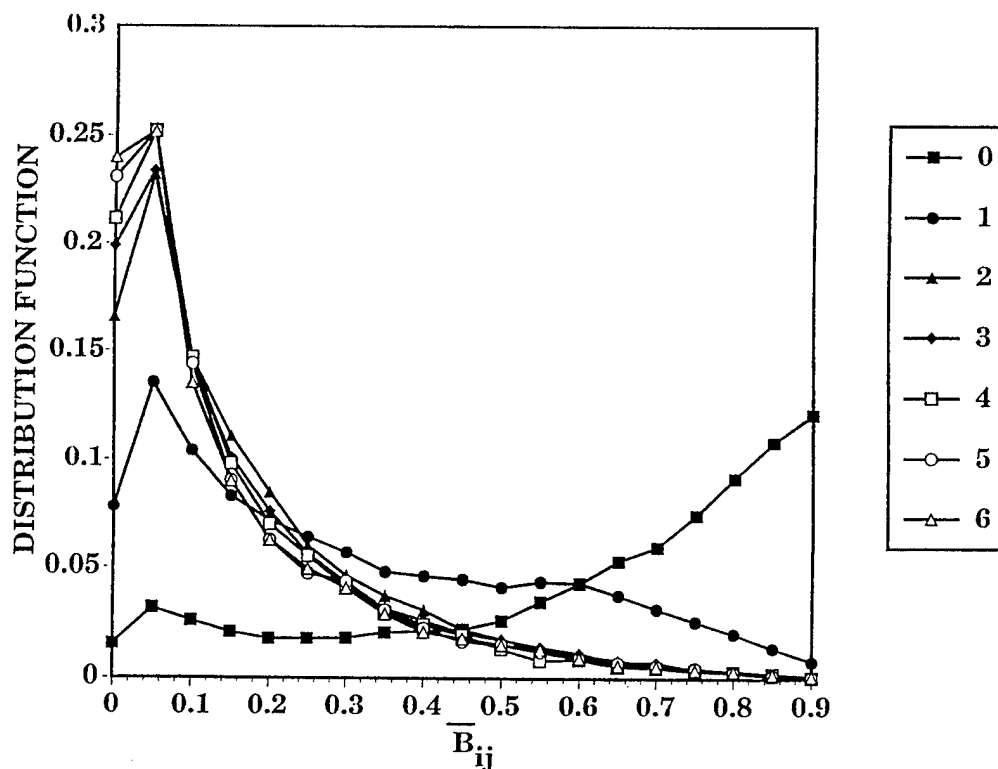


Figure 11. Normalized distribution of $\overline{B_{ij}}$ terms of Equation (2) of original A-B pairs for seven regions directly behind the shock front through the 12 km/s simulation (up to 7.8 ps). See text for definition of regions.

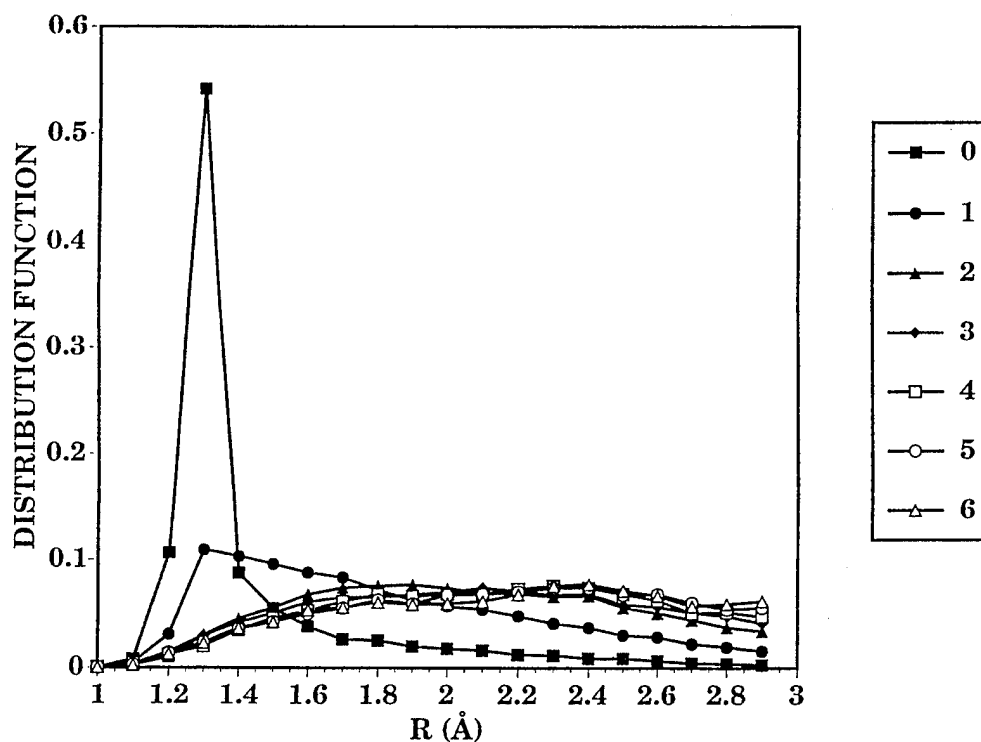


Figure 12. Normalized distribution of internuclear distances of original A-B pairs for seven regions directly behind the shock front through the 12 km/s simulation (up to 7.8 ps). See text for definition of regions.

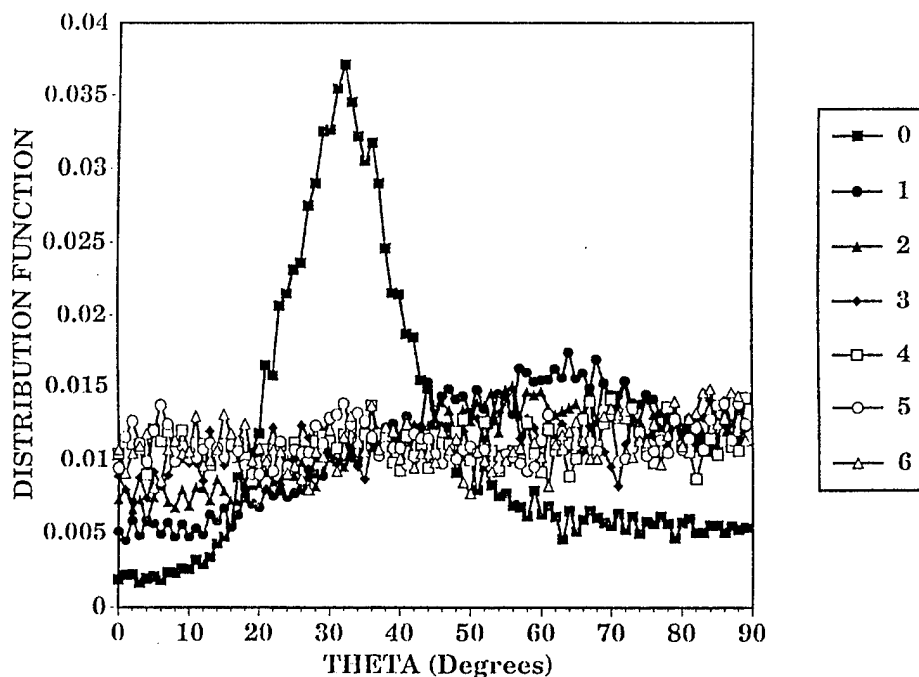


Figure 13. Normalized distribution of orientation angles of original A-B pairs relative to the crystal x-axis for seven regions directly behind the shock front through the 12 km/s simulation (up to 7.8 ps). See text for definition of regions.

have $\overline{B_{ij}}$ values > 0.7 within region 0. The distribution of $\overline{B_{ij}}$ values within region 1 is substantially different from that of region 0, with its peak at 0.1, but with a broad shoulder extending to 0.9. The average $\overline{B_{ij}}$ value within this region is 0.3, and the corresponding average internuclear distance is 1.8 Å. The distribution of R_{ABs} , however, shows a peak at 1.35 Å, with a broad shoulder extending to the dissociation limit of 3.0 Å. The intramolecular attraction for a $\overline{B_{ij}}$ value of 0.3 is slight (< -0.05 eV at $R(eq) = 2.0$ Å), and the distribution of internuclear distances suggests that a substantial number of A-B molecules experience no attraction and some degree of repulsion within this zone, also reflected in the distribution of the intramolecular interactions in Figure 10 for region 1. Beyond region 1, the $\overline{B_{ij}}$ distributions are similar, with peaks at 0.05. Likewise, the internuclear distance distributions are similar, and are broad bands extending from 1.2 Å to the dissociation limit of 3.0 Å.

Figure 13 shows the distribution of the orientation angle of the A-B molecules throughout the reaction zone. Structure in the orientational distributions exists in regions 0–2. In the undisturbed crystal, the molecular bond orientation is $\pm 29^\circ$ relative to the crystal x-axis. The distribution of the angular orientation in region 0 is peaked at 30° , indicating, for the most part, no rotational reorientation upon shock impact. This, coupled with the internuclear distance distribution for the A-B molecules (Figure 12) and the density of the system for this region (~ 7 amu/Å²) (Rice et al., in press), indicates that the first

geometric parameters affected by the shock wave are the intermolecular distances (they are reduced). By region 1, however, the angular orientational distribution has a broad peak at 60° , showing that the A-B molecules are lining up such that the molecular-bond axes are nearly perpendicular to the direction of the shock wave propagation. By region 3, the orientational distribution is flat, indicating that the original A-B pairs have experienced complete rotational disorder. By this region, atomization of the species has occurred and the atoms are energetically free to associate with potential molecular partners. We wish to point out that compression of the herringbone lattice in the direction of shock propagation, followed by realignment of the molecular-bond axes approximately perpendicular to this direction places the unreacted A-B molecules in an optimum arrangement to form the homonuclear products. As shown previously, the properties of the intramolecular interaction potentials for both heteronuclear and homonuclear interactions are such that at any degree of density, homonuclear attractions are greater than heteronuclear and homonuclear repulsions are less than heteronuclear. It is possible that the compression followed by realignment of the molecules initially behind the shock front might play some role in the rapidity with which energy redistribution among all modes and completion of reactions have occurred.

These results clearly indicate that A-B molecules within the reaction zone are transitioning to an atomic phase due to the changes in the intramolecular interactions caused by the high density behind the shock front. From as close as 2.0 \AA behind the shock front, the A-B molecules experience, on average, repulsive interactions. Therefore, we have a picture of A atoms and B atoms that are in close proximity to one another, but are not bound. For the regions beyond 0 and 1, the average $\overline{B_{ij}}$ values and corresponding distributions show little internuclear attraction whatsoever among the atoms, indicating complete atomization of the products. As the shock front proceeds through the crystal, the rarefying flow becomes less dense, increasing the $\overline{B_{ij}}$ values. Correspondingly, the repulsive intramolecular interactions decrease while attractions increase. Because the well depths of the homonuclear species are larger than that of the heteronuclear molecules, homonuclear product formation is energetically favored; the realignment of the molecules in region 1 puts the system in optimum orientation for homonuclear product formation. All of these factors result in complete reaction of the shocked A-B molecular crystal to exothermically form the homonuclear diatomic products.

Atomization of a molecular solid subjected to hydrostatic high pressure is not unknown. Such phenomena have been observed in high-pressure studies of atomization of solid iodine (Takemura et al. 1980, 1982; Fujii et al. 1987) HI (van Straaten and Silvera 1986), and IBr (Fujii 1985). Although pressure-induced atomization was not specifically investigated in a shock-loading experiment of iodine

(Alder and Christian 1960; McMahan, Hord, and Ross 1977), x-ray spectra taken from these experiments are consistent with the x-ray spectra of the atomized phase of solid iodine at pressures above 21 GPa (Takemura et al. 1980). *Ab initio* pseudopotential calculations have shown pressure-induced changes in electronic structure of molecular crystals, including loss of covalency leading to molecular dissociation with increasing pressure (McMahan 1986). Electron densities of these materials (Br_2 , I_2 , IBr) determined from x-ray diffraction studies as a function of pressure also show delocalization of the covalent electrons (Fujii 1995). These rearrangements of the electrons are consistent with the present study and provide the mechanism for the transition from a molecular solid to the atomized solid in several halogen materials. Experimental studies of energetic materials subjected to high pressure have shown that pressure can drastically affect thermal decomposition rates and reaction mechanisms (Piermarini, Block, and Miller 1987, 1989). For example, the activation energy for the thermal decomposition of β -HMX (octahydro-1,3,5,7-tetranitro-1,3,5,7-tetrazocine), one of the most widely used explosives, approaches zero at very high pressures (Piermarini, Block, and Miller 1987). This was attributed to changes in the interaction potential (i.e., electronic structure) of the system under compression. Similarly, the thermal rate of decomposition of nitromethane, a prototypical explosive, and its chemical reactivity were enhanced with increased pressure (Piermarini, Block, and Miller 1989). These studies, both experimental and theoretical, on real molecular crystals indicate changes in the electronic structure of molecular bonds due to pressure and suggest to us that the pressure-induced atomization mechanism of detonation for our model energetic crystal is not unreasonable. We stress, however, that the interaction potential for our system was not developed or parameterized to yield measured high-pressure behavior. Rather, the reaction mechanism (pressure-induced atomization) is a result of the functional form and choice of parameters for the potential. It may be that this model fortuitously describes correctly a significant reaction mechanism occurring in a detonation. The molecules used in the present study are very simple, containing but a single degree of vibrational motion. It will be interesting to investigate, with these techniques, the effect of large molecules (many vibrational modes) on the energy-sharing process and their importance on the reaction mechanisms. It is imperative that either new experimental techniques be developed to probe microscopically the state of the system behind a detonation wave or first-principles calculations such as those done by McMahan (1986) must be carried out to determine quantitatively the changes in the electronic structure of explosives when subjected to pressures consistent with those measured in detonations. Only then will it be possible to state whether models such as that presented in this work are adequate to represent correctly the chemical reactions leading to detonation.

5. CONCLUSIONS

We have presented a comparative study of models that produce features of an unsupported detonation. The three interaction potentials, based on Abell (1985) and Tersoff's (1988) ideas and developed by Brenner (1992, 1993), Robertson et al. (1992), and White et al. (1992, 1994), incorporate many-body effects on the intramolecular terms. A many-body term attenuates the molecular attractions with increasing density while increasing the repulsive portion of the term. This changes the equilibrium molecular size and binding energy of a molecule upon density increases. When the density becomes large enough, the atoms in molecule are pushed apart and feel no attraction. In other words, this model predicts pressure-induced atomization.

Results of a two-dimensional molecular-dynamics simulation of a detonation in an accompanying study show that for flyer plates moving with velocities greater than 4.7 km/s, unsupported detonations are sustained, and have similar macroscopic properties once the detonation waves reach the steady-state velocity (Rice et al., in press). The detonation wave propagates through the quiescent crystal at 6.6 km/s; immediately behind the detonation wave, there is, on average, a 14-Å-wide region in which microscopic and macroscopic properties of the crystal are time independent. It is within this region that the heteronuclear molecules are undergoing reaction; we have labeled this the reaction zone.

We examined in detail seven regions within the 14-Å-reaction zone over time; cumulative distributions of molecular properties including translational and internal KEs, geometric parameters, and intramolecular potential energies were calculated. The average values of properties of the reaction zone converge to time-independent, constant values approximately 4 Å behind the shock front. Within the 4-Å region immediately behind the shock front, the shock wave first compresses the crystal and rotates the molecules such that the molecular bonds are almost perpendicular to the shock wave propagation. Translational modes of the molecules are excited, but the internal modes of the molecules are cold. Thereafter, energy rapidly transfers into internal modes until an equipartitioning among these kinetic degrees of freedom are established. By this point, the atoms experience an almost completely repulsive intramolecular interaction; in other words, they become atomized. As the shock wave passes, the density in the rarefying flow becomes lower; concurrently the molecular bonding attractions increase, resulting in the association of the atoms to diatomic products. The attractive portions of the homonuclear interaction potentials are considerably larger than the heteronuclear interaction potential; thus, homonuclear product formation is energetically favored over heteronuclear recombination. The homonuclear association reactions release

substantial chemical energy which drives the detonation wave. Vibrational excitation of the reactant heteronuclear molecules to dissociation (thermal decomposition) does not contribute to the detonation mechanism. Rather, the mechanism of detonation for this model is pressure-induced atomization of the molecules behind the shock front, followed by association of the atoms to form homonuclear products. This mechanism is attributed directly to the functional form of the many-body term of the interaction potential; subsequent first-principles calculations must be done on systems subjected to high pressures to determine if this interaction potential correctly describes a significant mechanism for initiation reactions in detonation.

6. REFERENCES

- Abell, G. C. Physical Review B. Vol. 31, p. 6184, 1985.
- Alder, B. J., and R. H. Christian. Physical Review Letters. Vol. 4, p. 450, 1960.
- Brenner, D. W., D. H. Robertson, M. L. Elert, and C. T. White. Physical Review Letters. Vol. 70, p. 2174, 1993.
- Brenner, D. W. Shock Compression of Condensed Matter. Edited by S. C. Schmidt, R. D. Dick, J. W. Forbes, and D. G. Tasker, Elsevier Science Publishers B. V., p. 115, 1992.
- Chen, S., W. A. Tolbert, and D. D. Dlott. Journal of Physical Chemistry. Vol. 98, p. 7759, 1994.
- Chen, S., X. Hong, J. R. Hill, and D. D. Dlott. Journal of Physical Chemistry. Vol. 99, p. 4525, 1995.
- Dlott, D. D., and M. D. Fayer. Journal of Chemical Physics. Vol. 92, p. 3798, 1990.
- Fickett, W., and W. C. Davis. Detonation. Berkeley, CA: University of California Press, 1979.
- Fickett, W. Introduction to Detonation. Berkeley, CA: University of California Press, 1985.
- Fried, L. E., and A. J. Ruggiero. Journal of Physical Chemistry. Vol. 98, p. 9786, 1994.
- Fujii, Y. Abstract 4m.4.D. American Crystallographic Association Annual Meeting, 1995.
- Fujii, Y., K. Hase, N. Hamaya, Y. Ohishi, A. Onodera, O. Shimomura, and K. Takemura. Physical Review Letters. Vol. 58, p. 796, 1987.
- Fujii, Y., Y. Ohishi, A. Onodera, K. Takemura, and R. L. Reichlin. Japanese Journal of Applied Physics. Vol. 24S, p. 606, 1985.
- Gupta, Y. M., G. I. Pangilinan, J. M. Winey, and C. P. Constantinou. Chemical Physics Letters. Vol. 232, p. 341, 1995.
- Karo, A. M., J. R. Hardy, and F. E. Walker. Acta Astronautica. Vol. 5, p. 1041, 1978.
- Kawakatsu, T., and A. Ueda. Journal of Physical Society of Japan. Vol. 57, p. 2955, 1988.
- Kawakatsu, T., and A. Ueda. Journal of Physical Society of Japan. Vol. 58, p. 831, 1989.
- Kawakatsu, T., T. Matsuda, and A. Ueda. Journal of Physical Society of Japan. Vol. 57, p. 1191, 1988.
- Margenau, H., and G. M. Murphy. The Mathematics of Physics and Chemistry. New York: Van Nostrand, pp. 476-477, 1943.
- McMahan, A. K., B. L. Hord, and M. Ross. Physical Review B. Vol. 15, p. 726, 1977.

- McMahan, A. K. Physica. Vol. 139 and 140 B, p. 31, 1986.
- Piermarini, G. J., S. Block, and P. J. Miller. Journal of Physical Chemistry. Vol. 91, p. 3872, 1987.
- Piermarini, G. J., S. Block, and P. J. Miller. Journal of Physical Chemistry. Vol. 93, p. 457, 1989.
- Rice, B. M., W. Mattson, J. Grosh, and S. F. Trevino. Physical Review E. In press.
- Robertson, D. H., D. W. Brenner, M. L. Elert, C. T. White. Shock Compression of Condensed Matter. Edited by S. C. Schmidt, R. D. Dick, J. W. Forbes, and D. G. Tasker, Elsevier Science Publishers B. V., p. 123, 1992.
- Takemura, K., S. Minomura, O. Shimomura, and Y. Fujii. Physical Review Letters. Vol. 45, p. 1881, 1980.
- Takemura, K., S. Minomura, O. Shimomura, Y. Fujii, and J. D. Axe. Physical Review B. Vol. 26, p. 998, 1982.
- Tersoff, J. Physical Review Letters. Vol. 61, p. 2879, 1988.
- Tokmakoff, A., M. D. Fayer, and D. D. Dlott. Journal of Physical Chemistry. Vol. 97, p. 1901, 1993.
- Tsai, D. H., and S. F. Trevino. Physical Review A. Vol. 24, p. 2743, 1981.
- van Straaten, J., and I. F. Silvera. Physical Review Letters. Vol. 57, p. 766, 1986.
- White, C. T., D. H. Robertson, M. L. Elert, and D. W. Brenner. Microscopic Simulations of Complex Hydrodynamic Phenomena. Edited by M. Mareschal and B. L. Holian, NY: Plenum Press, p. 111, 1992.
- White, C. T., S. B. Sinnott, J. W. Mintmire, D. W. Brenner, and D. H. Robertson. International Journal of Quantum Chemical Symposium. Vol. 28, p. 129, 1994.

<u>NO. OF COPIES</u>	<u>ORGANIZATION</u>
2	DEFENSE TECHNICAL INFO CTR ATTN DTIC DDA 8725 JOHN J KINGMAN RD STE 0944 FT BELVOIR VA 22060-6218

1	DIRECTOR US ARMY RESEARCH LAB ATTN AMSRL OP SD TA 2800 POWDER MILL RD ADELPHI MD 20783-1145
---	---------------------------------------------------------------------------------------------------------

3	DIRECTOR US ARMY RESEARCH LAB ATTN AMSRL OP SD TL 2800 POWDER MILL RD ADELPHI MD 20783-1145
---	---------------------------------------------------------------------------------------------------------

1	DIRECTOR US ARMY RESEARCH LAB ATTN AMSRL OP SD TP 2800 POWDER MILL RD ADELPHI MD 20783-1145
---	---------------------------------------------------------------------------------------------------------

ABERDEEN PROVING GROUND

5	DIR USARL ATTN AMSRL OP AP L (305)
---	---------------------------------------

<u>NO. OF COPIES</u>	<u>ORGANIZATION</u>
1	HQDA ATTN SARD TT DR F MILTON PENTAGON WASHINGTON DC 20310-0103
1	HQDA ATTN SARD TT MR J APPEL PENTAGON WASHINGTON DC 20310-0103
1	HQDA OASA RDA ATTN DR C H CHURCH PENTAGON ROOM 3E486 WASHINGTON DC 20310-0103
4	COMMANDER US ARMY RESEARCH OFFICE ATTN R GHIRARDELLI D MANN R SINGLETON R SHAW P O BOX 12211 RSCH TRNGLE PK NC 27709-2211
1	DIRECTOR ARMY RESEARCH OFFICE ATTN AMXRO RT IP LIB SERVICES P O BOX 12211 RSCH TRNGLE PK NC 27709-2211
2	COMMANDER US ARMY ARDEC ATTN SMCAR AEE B D S DOWNS PCTNY ARSNL NJ 07806-5000
2	COMMANDER US ARMY ARDEC ATTN SMCAR AEE J A LANNON PCTNY ARSNL NJ 07806-5000
1	COMMANDER US ARMY ARDEC ATTN SMCAR AEE BR L HARRIS PCTNY ARSNL NJ 07806-5000
2	COMMANDER US ARMY MISSILE COMMAND ATTN AMSMI RD PR E A R MAYKUT AMSMI RD PR P R BETTS REDSTONE ARSENAL AL 35809

<u>NO. OF COPIES</u>	<u>ORGANIZATION</u>
1	OFFICE OF NAVAL RESEARCH DEPARTMENT OF THE NAVY ATTN R S MILLER CODE 432 800 N QUINCY STREET ARLINGTON VA 22217
1	COMMANDER NAVAL AIR SYSTEMS COMMAND ATTN J RAMNARACE AIR 54111C WASHINGTON DC 20360
2	COMMANDER NAVAL SURFACE WARFARE CENTER ATTN R BERNECKER R 13 G B WILMOT R 16 SILVER SPRING MD 20903-5000
5	COMMANDER NAVAL RESEARCH LABORATORY ATTN M C LIN J MCDONALD E ORAN J SHNUR R J DOYLE CODE 6110 WASHINGTON DC 20375
2	COMMANDER NAVAL WEAPONS CENTER ATTN T BOGGS CODE 388 T PARR CODE 3895 CHINA LAKE CA 93555-6001
1	SUPERINTENDENT NAVAL POSTGRADUATE SCHOOL DEPT OF AERONAUTICS ATTN D W NETZER MONTEREY CA 93940
3	AL LSCF ATTN R CORLEY R GEISLER J LEVINE EDWARDS AFB CA 93523-5000
1	AFOSR ATTN J M TISHKOFF BOLLING AIR FORCE BASE WASHINGTON DC 20332

NO. OF
COPIES ORGANIZATION

1 OSD SDIO IST
ATTN L CAVENY
PENTAGON
WASHINGTON DC 20301-7100

1 COMMANDANT
USAFAS
ATTN ATSF TSM CN
FORT SILL OK 73503-5600

1 UNIV OF DAYTON RSCH INSTITUTE
ATTN D CAMPBELL
AL PAP
EDWARDS AFB CA 93523

1 NASA
LANGLEY RESEARCH CENTER
ATTN G B NORTHAM MS 168
LANGLEY STATION
HAMPTON VA 23365

4 NATIONAL BUREAU OF STANDARDS
US DEPARTMENT OF COMMERCE
ATTN J HASTIE
M JACOX
T KASHIWAGI
H SEMERJIAN
WASHINGTON DC 20234

2 DIRECTOR
LAWRENCE LIVERMORE NATIONAL LAB
ATTN C WESTBROOK
W TAO MS L 282
P O BOX 808
LIVERMORE CA 94550

1 DIRECTOR
LOS ALAMOS NATIONAL LAB
ATTN B NICHOLS T7 MS B284
P O BOX 1663
LOS ALAMOS NM 87545

2 PRINCETON COMBUSTION
RESEARCH LABORATORIES INC
ATTN N A MESSINA
M SUMMERFIELD
PRINCETON CORPORATE PLAZA
BLDG IV SUITE 119
11 DEERPARK DRIVE
MONMOUTH JUNCTION NJ 08852

NO. OF
COPIES ORGANIZATION

3 DIRECTOR
SANDIA NATIONAL LABORATORIES
DIVISION 8354
ATTN S JOHNSTON
P MATTERN
D STEPHENSON
LIVERMORE CA 94550

1 BRIGHAM YOUNG UNIVERSITY
DEPT OF CHEMICAL ENGINEERING
ATTN M W BECKSTEAD
PROVO UT 84058

1 CALIFORNIA INSTITUTE OF TECH
JET PROPULSION LABORATORY
ATTN L STRAND MS 125 224
4800 OAK GROVE DRIVE
PASADENA CA 91109

1 CALIFORNIA INSTITUTE OF TECHNOLOGY
ATTN F E C CULICK MC 301 46
204 KARMAN LAB
PASADENA CA 91125

1 UNIVERSITY OF CALIFORNIA
LOS ALAMOS SCIENTIFIC LAB
P O BOX 1663 MAIL STOP B216
LOS ALAMOS NM 87545

1 UNIVERSITY OF CALIFORNIA BERKELEY
CHEMISTRY DEPARMENT
ATTN C BRADLEY MOORE
211 LEWIS HALL
BERKELEY CA 94720

1 UNIVERSITY OF CALIFORNIA SAN DIEGO
ATTN F A WILLIAMS
AMES B010
LA JOLLA CA 92093

2 UNIV OF CALIFORNIA SANTA BARBARA
QUANTUM INSTITUTE
ATTN K SCHOFIELD
M STEINBERG
SANTA BARBARA CA 93106

1 UNIV OF COLORADO AT BOULDER
ENGINEERING CENTER
ATTN J DAILY
CAMPUS BOX 427
BOULDER CO 80309-0427

<u>NO. OF COPIES</u>	<u>ORGANIZATION</u>
3	UNIV OF SOUTHERN CALIFORNIA DEPT OF CHEMISTRY ATTN R BEAUDET S BENSON C WITTIG LOS ANGELES CA 90007
1	CORNELL UNIVERSITY DEPARTMENT OF CHEMISTRY ATTN T A COOL BAKER LABORATORY ITHACA NY 14853
1	UNIVERSITY OF DELAWARE CHEMISTRY DEPARTMENT ATTN T BRILL NEWARK DE 19711
1	UNIVERSITY OF FLORIDA DEPT OF CHEMISTRY ATTN J WINEFORDNER GAINESVILLE FL 32611
3	GEORGIA INSTITUTE OF TECHNOLOGY SCHOOL OF AEROSPACE ENGINEERING ATTN E PRICE W C STRAHLE B T ZINN ATLANTA GA 30332
1	UNIVERSITY OF ILLINOIS DEPT OF MECH ENG ATTN H KRIER 144MEB 1206 W GREEN ST URBANA IL 61801
1	THE JOHNS HOPKINS UNIV CPIA ATTN T W CHRISTIAN 10630 LITTLE PATUXENT PKWY SUITE 202 COLUMBIA MD 21044-3200
1	UNIVERSITY OF MICHIGAN GAS DYNAMICS LAB ATTN G M FAETH AEROSPACE ENGINEERING BLDG ANN ARBOR MI 48109-2140
1	UNIVERSITY OF MINNESOTA DEPT OF MECHANICAL ENGINEERING ATTN E FLETCHER MINNEAPOLIS MN 55455

<u>NO. OF COPIES</u>	<u>ORGANIZATION</u>
4	PENNSYLVANIA STATE UNIVERSITY DEPT OF MECHANICAL ENGINEERING ATTN K KUO M MICCI S THYNELL V YANG UNIVERSITY PARK PA 16802
2	PRINCETON UNIVERSITY FORRESTAL CAMPUS LIBRARY ATTN K BREZINSKY I GLASSMAN P O BOX 710 PRINCETON NJ 08540
1	PURDUE UNIVERSITY SCHL OF AERONAUTICS & ASTRONAUTICS ATTN J R OSBORN GRISSOM HALL WEST LAFAYETTE IN 47906
1	PURDUE UNIVERSITY DEPARTMENT OF CHEMISTRY ATTN E GRANT WEST LAFAYETTE IN 47906
2	PURDUE UNIVERSITY SCHL OF MECHANICAL ENGNRNG ATTN N M LAURENDEAU S N B MURTHY TSPC CHAFFEE HALL WEST LAFAYETTE IN 47906
1	RENSSELAER POLYTECHNIC INST DEPT OF CHEMICAL ENGINEERING ATTN A FONTJN TROY NY 12181
1	STANFORD UNIVERSITY DEPT OF MECHANICAL ENGINEERING ATTN R HANSON STANFORD CA 94305
1	UNIVERSITY OF TEXAS DEPT OF CHEMISTRY ATTN W GARDINER AUSTIN TX 78712
1	VA POLYTECH INST AND STATE UNIV ATTN J A SCHETZ BLACKSBURG VA 24061

<u>NO. OF COPIES</u>	<u>ORGANIZATION</u>
1	APPLIED COMBUSTION TECHNOLOGY INC ATTN A M VARNEY P O BOX 607885 ORLANDO FL 32860
2	APPLIED MECHANICS REVIEWS ASME ATTN R E WHITE & A B WENZEL 345 E 47TH STREET NEW YORK NY 10017
1	TEXTRON DEFENSE SYSTEMS ATTN A PATRICK 2385 REVERE BEACH PARKWAY EVERETT MA 02149-5900
1	BATTELLE TWSTIAC 505 KING AVENUE COLUMBUS OH 43201-2693
1	COHEN PROFESSIONAL SERVICES ATTN N S COHEN 141 CHANNING STREET REDLANDS CA 92373
1	EXXON RESEARCH & ENG CO ATTN A DEAN ROUTE 22E ANNANDALE NJ 08801
1	GENERAL APPLIED SCIENCE LABS INC 77 RAYNOR AVENUE RONKONKAMA NY 11779-6649
1	GENERAL ELECTRIC ORDNANCE SYSTEMS ATTN J MANDZY 100 PLASTICS AVENUE PITTSFIELD MA 01203
1	GENERAL MOTORS RSCH LABS PHYSICAL CHEMISTRY DEPARTMENT ATTN T SLOANE WARREN MI 48090-9055
2	HERCULES INC ATTN W B WALKUP E A YOUNT P O BOX 210 ROCKET CENTER WV 26726

<u>NO. OF COPIES</u>	<u>ORGANIZATION</u>
1	HERCULES INC ATTN R V CARTWRIGHT 100 HOWARD BLVD KENVIL NJ 07847
1	ALLIANT TECHSYSTEMS INC MARINE SYSTEMS GROUP ATTN D E BRODEN MS MN50 2000 600 2ND STREET NE HOPKINS MN 55343
1	ALLIANT TECHSYSTEMS INC ATTN R E TOMPKINS MN 11 2720 600 SECOND ST NORTH HOPKINS MN 55343
1	IBM CORPORATION RESEARCH DIVISION ATTN A C TAM 5600 COTTLE ROAD SAN JOSE CA 95193
1	IIT RESEARCH INSTITUTE ATTN R F REMALY 10 WEST 35TH STREET CHICAGO IL 60616
1	LOCKHEED MISSILES & SPACE CO ATTN GEORGE LO 3251 HANOVER STREET DEPT 52 35 B204 2 PALO ALTO CA 94304
1	OLIN ORDNANCE ATTN V MCDONALD LIBRARY P O BOX 222 ST MARKS FL 32355-0222
1	PAUL GOUGH ASSOCIATES INC ATTN P S GOUGH 1048 SOUTH STREET PORTSMOUTH NH 03801-5423
1	HUGHES AIRCRAFT COMPANY ATTN T E WARD PO BOX 11337 TUCSON AZ 85734-1337

<u>NO. OF COPIES</u>	<u>ORGANIZATION</u>
1	SCIENCE APPLICATIONS INC ATTN R B EDELMAN 23146 CUMORAH CREST WOODLAND HILLS CA 91364
3	SRI INTERNATIONAL ATTN G SMITH D CROSLEY D GOLDEN 333 RAVENSWOOD AVENUE MENLO PARK CA 94025
1	STEVENS INSTITUTE OF TECH DAVIDSON LABORATORY ATTN R MCALEVY III HOBOKEN NJ 07030
1	SVERDRUP TECHNOLOGY INC LERC GROUP ATTN R J LOCKE MS SVR 2 2001 AEROSPACE PARKWAY BROOK PARK OH 44142
1	SVERDRUP TECHNOLOGY INC ATTN J DEUR 2001 AEROSPACE PARKWAY BROOK PARK OH 44142
3	THIOKOL CORPORATION ELKTON DIVISION ATTN R BIDDLE R WILLER TECH LIB P O BOX 241 ELKTON MD 21921
3	THIOKOL CORPORATION WASATCH DIVISION ATTN S J BENNETT P O BOX 524 BRIGHAM CITY UT 84302
1	UNITED TECHNOLOGIES RSCH CENTER ATTN A C ECKBRETH EAST HARTFORD CT 06108
1	UNITED TECHNOLOGIES CORP CHEMICAL SYSTEMS DIVISION ATTN R R MILLER P O BOX 49028 SAN JOSE CA 95161-9028

<u>NO. OF COPIES</u>	<u>ORGANIZATION</u>
1	UNIVERSAL PROPULSION COMPANY ATTN H J MCSPADDEN 25401 NORTH CENTRAL AVENUE PHOENIX AZ 85027-7837
1	VERITAY TECHNOLOGY INC ATTN E B FISHER 4845 MILLERSPORT HIGHWAY EAST AMHERST NY 14051-0305
1	FREEDMAN ASSOCIATES ATTN E FREEDMAN 2411 DIANA ROAD BALTIMORE MD 21209-1525
3	ALLIANT TECHSYSTEMS ATTN C CANDLAND L OSGOOD R BECKER 600 SECOND ST NE HOPKINS MN 55343
1	DIRECTOR US ARMY BENET LABS ATTN SAM SOPOK AMSTA AR CCB T WATERVLIET NY 12189

NO. OF
COPIES ORGANIZATION

ABERDEEN PROVING GROUND

36 DIR USARL
ATTN: AMSRL-WT-P, A HORST
AMSRL-WT-PC,
R A FIFER
G F ADAMS
W R ANDERSON
R A BEYER
S W BUNTE
C F CHABALOWSKI
K P MCNEILL-BOONSTOPPEL
A COHEN
R CUMPTON
R DANIEL
D DEVYNCK
N F FELL
B E FORCH
J M HEIMERL
A J KOTLAR
M R MANAA
W F MCBRATNEY
K L MCNESBY
S V MEDLIN
M S MILLER
A W MIZIOLEK
S H MODIANO
J B MORRIS
J E NEWBERRY
S A NEWTON
R A PESCE-RODRIGUEZ
B M RICE
R C SAUSA
M A SCHROEDER
J A VANDERHOFF
M WENSING
A WHREN
J M WIDDER
C WILLIAMSON
AMSRL-CI-CA, R PATEL

INTENTIONALLY LEFT BLANK.

USER EVALUATION SHEET/CHANGE OF ADDRESS

This Laboratory undertakes a continuing effort to improve the quality of the reports it publishes. Your comments/answers to the items/questions below will aid us in our efforts.

1. ARL Report Number ARL-TR-982 Date of Report March 1996

2. Date Report Received _____

3. Does this report satisfy a need? (Comment on purpose, related project, or other area of interest for which the report will be used.) _____

4. Specifically, how is the report being used? (Information source, design data, procedure, source of ideas, etc.) _____

5. Has the information in this report led to any quantitative savings as far as man-hours or dollars saved, operating costs avoided, or efficiencies achieved, etc? If so, please elaborate. _____

6. General Comments. What do you think should be changed to improve future reports? (Indicate changes to organization, technical content, format, etc.) _____

CURRENT
ADDRESS

Organization

Name

Street or P.O. Box No.

City, State, Zip Code

7. If indicating a Change of Address or Address Correction, please provide the Current or Correct address above and the Old or Incorrect address below.

OLD
ADDRESS

Organization

Name

Street or P.O. Box No.

City, State, Zip Code

(Remove this sheet, fold as indicated, tape closed, and mail.)
(DO NOT STAPLE)

DEPARTMENT OF THE ARMY

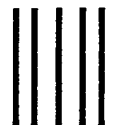
OFFICIAL BUSINESS

BUSINESS REPLY MAIL

FIRST CLASS PERMIT NO 0001,APG,MD

POSTAGE WILL BE PAID BY ADDRESSEE

DIRECTOR
U.S. ARMY RESEARCH LABORATORY
ATTN: AMSRL-WT-PC
ABERDEEN PROVING GROUND, MD 21005-5066



NO POSTAGE
NECESSARY
IF MAILED
IN THE
UNITED STATES

